Journal of Biomolecular NMR, **25:** 291–311, 2003.
KLUWER/ESCOM

A strategy to obtain backbone resonance assignments of deuterated proteins in the presence of incomplete amide $^{2}H/^{1}H$ back-exchange

Frank Löhr*, Vicky Katsemi, Judith Hartleib, Ulrich Günther & Heinz Rüterjans
Johann Wolfgang Goethe-University Frankfurt, Center for Biomolecular Magnetic Resonance, Institute of Biophysical Chemistry, Marie Curie-Strasse 9, N230, 1.OG, D-60439 Frankfurt, Germany

Received 29 October 2002; Accepted 21 November 2002

Key words: DFPase, fractional deuteration, multiple-quantum line narrowing, slow D/H exchange, triple-resonance NMR, TROSY

Abstract

Replacement of non-exchangeable protons by deuterons has become a standard tool in structural studies of proteins on the order of 30–40 kDa to overcome problems arising from rapid ^{1}H and ^{13}C transverse relaxation. However, ^{1}H nuclei are required at exchangeable sites to maintain the benefits of proton detection. Protein expression in D_2O-based media containing deuterated carbon sources yields protein deuterated in all positions. Subsequent D/H-exchange is commonly used to reintroduce protons in labile positions. Since this strategy may fail for large proteins with strongly inhibited exchange we propose to express the protein in fully deuterated algal lysate medium in 100% H_2O. As a side-effect partial C^{α} protonation occurs in a residue-type dependent manner. Samples obtained by this protocol are suitable for complementary $^{1}H^{N}$- and $^{1}H^{\alpha}$-based triple resonance experiments allowing complete backbone resonance assignments in cases where back-exchange of amide protons is very slow after expression in D_2O and refolding of chemically denatured protein is not feasible. This approach is explored using a 35-kDa protein as a test case. The degree of C^{α} protonation of individual amino acids is determined quantitatively and transverse relaxation properties of $^{1}H^{N}$ and ^{15}N nuclei of the partially deuterated protein are investigated and compared to the fully protonated and perdeuterated species. Based on the deviations of assigned chemical shifts from random coil values its solution secondary structure can be established.

Introduction

Deuteration has effectively extended the size limit of proteins amenable to structural studies by solution NMR (LeMaster, 1994; Sattler and Fesik, 1996; Arrowsmith and Wu, 1998; Farmer II and Venters, 1998; Gardner and Kay, 1998). The elimination of the efficient ^{1}H-^{1}H and ^{1}H-^{13}C dipolar spin relaxation pathways as well as ^{1}H-^{1}H scalar couplings in $^{2}H/^{13}C/^{15}N$-labelled proteins, in combination with ^{2}H decoupling (Grzesiek et al., 1993; Kushlan and LeMaster, 1993; Yamazaki et al., 1994; Farmer II and Venters, 1995; Shan et al., 1996), results in dramatic improvements of amide-proton detected triple-resonance experiments in terms of both sensitivity and resolution. The destructive interference of the remaining dominant contributions to relaxation, $^{1}H^{N}$-^{15}N dipole-dipole coupling (DD) and $^{1}H^{N}$ or ^{15}N chemical shift anisotropy (CSA), which is exploited in [^{15}N, ^{1}H]-TROSY (Pervushin et al., 1997) based triple-resonance methods further enhances the advantages of deuteration, allowing sequential resonance assignments of large proteins to be obtained (Salzmann et al., 1998, 1999a, 2000; Yang and Kay, 1999a; Konrat et al., 1999; Loria et al., 1999; Mulder et al., 2000; Tugarinov et al., 2002).

While high deuteration levels of nonexchangeable sites in a protein are beneficial for main chain assignment experiments, the vast majority of pulse sequences designed for this purpose employ proton detection for sensitivity reasons. This requires back-exchange of amide protons after protein expression us-

*To whom correspondence should be addressed. E-mail: murph@bpc.uni-frankfurt.de

ing D_2O-based bacterial growth media. In favourable cases this process is completed after isolation and purification of the protein taking place in H_2O-based buffers. However, amides involved in strong hydrogen bonds or buried inside the protein and thus not accessible to the solvent may remain deuterated. Unfolding of the protein using chemical denaturants followed by refolding in the presence of H_2O can solve this problem (Venters et al., 1996; Constantine et al., 1997) but may not always be feasible. In this situation, random fractional deuteration (LeMaster and Richards, 1988; Nietlispach et al., 1996) achieved by growing bacteria in minimal media with the D_2O/H_2O ratio adjusted to the desired level of deuterium incorporation, is not a useful alternative, because the degree of protonation at slowly exchanging amide sites is at most as high as that of carbon sites, compromising the efficiency of triple-resonance pulse sequences due to the reintroduction of ^1H-^1H and ^1H-^{13}C DD interactions.

As an example for an unfavourable case, the monomeric 314-residue (MW = 35 kDa) protein diisopropylfluorophosphatase (DFPase; EC 3.1.8.2.), which is currently being investigated in our laboratory (Hartleib and Rüterjans, 2001a, b; Hartleib et al., 2001; Scharff et al., 2001), exhibits very slow D/H exchange at a substantial fraction of its backbone amides. This enzyme, initially isolated from the head ganglion of the squid *Loligo vulgaris*, hydrolyzes diisopropylfluorophosphate (DFP) and a wide variety of chemical warfare agents, including sarin, soman and tabun, while no natural substrate of physiological role has yet been identified. Preliminary NMR studies using a $^{13}C/^{15}N$-labelled protein sample revealed that the most sensitive triple-resonance experiments, HNCO and HNCA (Ikura et al., 1990; Grzesiek and Bax, 1992a), were of acceptable quality when recorded as [^{15}N, ^1H]-TROSY versions (Salzmann et al., 1998), whereas crucial experiments involving ^{13}C-^{13}C transfers such as [^{15}N, ^1H]-TROSY-HNCACB (Wittekind and Mueller, 1993; Salzmann et al., 1999a) or [^{15}N, ^1H]-TROSY-HN(CA)CO (Clubb et al., 1992; Salzmann et al., 1999a) failed. Due to extensive $^{13}C^{\alpha}$ chemical shift degeneracies in a 314-residue protein it is inconceivable to obtain sequential assignments exclusively based on connectivites observed in the HNCA. To obtain HNCACB and HN(CA)CO-type spectra deuteration is required to improve relaxation properties. However, as illustrated in Figure 1, a perdeuterated sample of DFPase in 95% H_2O/5% D_2O lacks approximately one third of the backbone amide protons that give rise to ^1H-^{15}N correlations

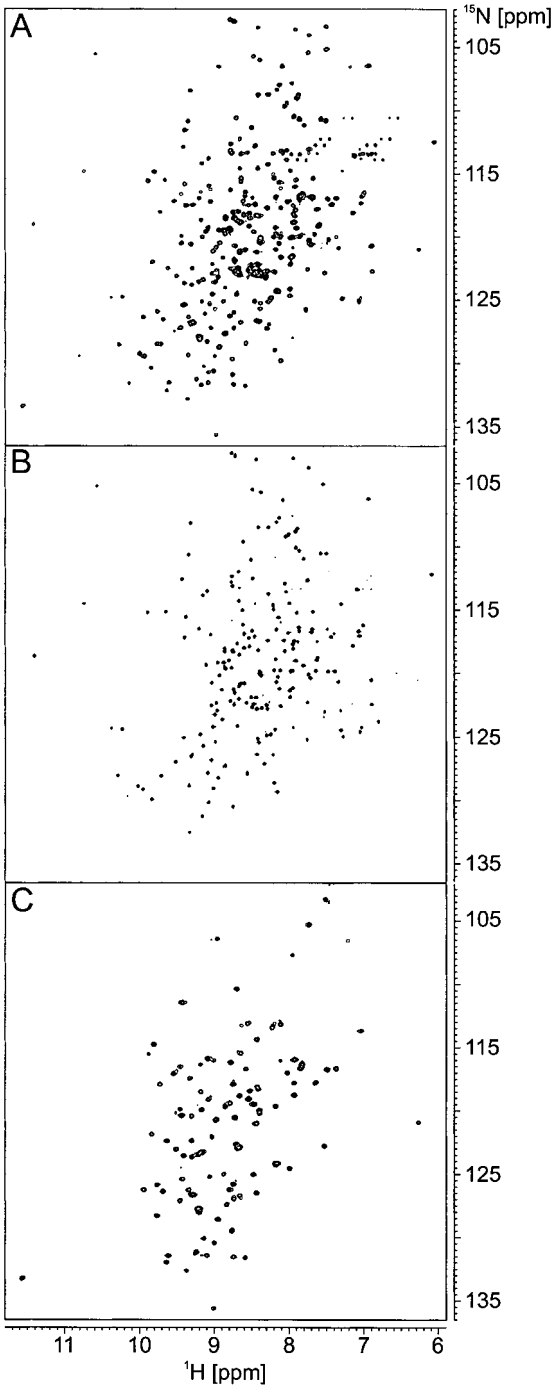

Figure 1. Amide regions of [^{15}N, ^1H]-TROSY spectra of DFPase from *Loligo vulgaris* demonstrating the very slow $^2H/^1H$ exchange at many of its amide sites. Samples used were (A) [U-98% ^{15}N]-labelled, dissolved in 95% H_2O/5% D_2O, (B) [U > 95% ^2H; U-98% ^{15}N]-labelled, dissolved in 95% H_2O/5% D_2O and (C) [U-98% ^{15}N]-labelled, dissolved in 99.9% D_2O. All spectra were recorded at 800 MHz with the temperature adjusted to 28 °C. Samples B and C were stored at room temperature for approximately eight weeks before data acquisition.

in a non-deuterated sample. Conversely, the missing amide signals can be detected in a spectrum of non-deuterated DFPase dissolved in 100% D_2O for several weeks. Even after a period as long as one year the number of unexchanged amide deuterons in a perdeuterated sample still amounts to 90 (data not shown). Unfortunately, all attempts to effect the back-exchange of deuterated amides in the perdeuterated sample by increasing temperature, pH or by addition of urea or guanidinium chloride were either ineffective or resulted in the irreversible denaturation of DFPase. Therefore a different ^2H enrichment strategy was pursued to enable more complete resonance assignments than would be achievable with either non- or perdeuterated samples.

Highly deuterated proteins with full protonation at all amide sites can be prepared by culturing *E. coli* in deuterated algal lysate in 100% H_2O. This procedure yields approximately 80% deuteration for methyl groups while the deuteration level at C^α sites is significantly lower due to the incorporation of water protons during biosynthesis of amino acids depleted during bacterial growth (Markus et al., 1994). Recently, a similar approach has been used to improve the spectral quality of 'in cell' NMR experiments, where back-exchange of amide protons cannot be effected by reversible denaturation of overexpressed proteins (Serber et al., 2001). The higher proton density compared to a perdeuterated sample involves less favourable relaxation properties, reducing sensitivity of $^1H^N$-directed triple-resonance experiments to some degree. On the other hand, the presence of α-protons provides independent means to obtain intraresidual and sequential connectivities within the protein backbone. Yamazaki et al. (1997) have introduced a suite of efficient $^1H^\alpha$-based triple-resonance pulse sequences taking advantage of $^1H^\alpha/^{13}C^\alpha$ multiple-quantum line-narrowing (Griffey and Redfield, 1987) to assign the backbone resonances of a slow tumbling protein. They obtained a selectively $^1H^\alpha$-, uniformly $^2H/^{13}C/^{15}N$-labelled protein using a medium containing a mixture of correspondingly labelled, chemically synthesized amino acids. To minimize ^1H-^1H DD interactions, the sample was dissolved in D_2O. In a very simple manner, the use of a fully deuterated algal lysate medium provides similarly labelled proteins which are, however, uniformly protonated at their amide sites, irrespective of the solvent exchange characteristics of the folded protein. This enables application of both H^N- and H^α-based 'out-and-back' type triple-resonance experiments as well as 'straight through' type sequences where α-protons are initially excited and amide protons finally detected. In this contribution we will use DFPase as an example to show how this strategy can be employed to achieve the main chain resonance assignment of larger proteins with 'unexchangeable' amide protons.

Materials and methods

Sample preparations

Recombinant DFPase from *Loligo vulgaris* was expressed in *E. coli* BL21 carrying the pKKHisND plasmid where the sequence was encoded as a fusion to a cleavable N-terminal His-tag. For the production of $^{13}C/^{15}N$- and ^{15}N-labelled protein, cells were grown on M9 minimal medium containing 1 g l^{-1} $^{15}NH_4Cl$ (99%) (Martek Biosciences Corp., Columbia, MD) as the sole nitrogen source and 1 g l^{-1} of either $^{13}C_6$ (> 98%) (Martek) or unlabelled glucose as well as 2.5 g l^{-1} of either $^{13}C_3$ (99%) (Martek) or unlabelled glycerol as carbon sources. Uniformly $^2H/^{13}C/^{15}N$-labelled DFPase was produced using a ^2H- (98%), ^{13}C- (97–98%) and ^{15}N- (96–99%) enriched algal lysate (Bio-Express-1000-CDN, Cambridge Isotope Laboratories, Inc., Andover, MA). The 10× concentrate of the medium was diluted (1:30) by 99.9% D_2O and supplemented with 1 g l^{-1} $^2H_7$ (> 97%), $^{13}C_6$ (> 98%) glucose (Martek) and 1 g l^{-1} $^{15}NH_4Cl$. The same algal lysate was employed to obtain a partially deuterated, $^{13}C/^{15}N$-labelled DFPase. Contrary to the protocol for the perdeuterated protein, the 10 × concentrated medium was diluted into H_2O (1:10) and no further carbon and nitrogen sources added. Expression was induced by addition of IPTG at an OD_{600} of 0.8, after which cells were grown overnight at a temperature of 30 °C. The isolation and purification of the protein was carried out as described previously (Hartleib and Rüterjans, 2001a). All NMR samples were dissolved in 10 mM 1,3-bis[tris-(hydroxymethyl-)methylamino]-propane (Bis-Tris-propane) buffer (95% H_2O/5% D_2O), pH = 6.5, containing 5 mM $CaCl_2$, 0.03% NaN_3 and 50 μg ml^{-1} Pefabloc protease inhibitor. A small amount of 3-(trimethylsilyl)-1-propanesulfonic acid (DSS) was added as internal standard. Protein concentrations of ^{15}N-, $^{13}C/^{15}N$-, $^2H/^{13}C/^{15}N$-labelled and partially deuterated, $^{13}C/^{15}N$-labelled samples were 1.0, 1.6, 0.9 and 0.6 mM, respectively. Samples were placed in Shigemi microcells with total volumes ranging from 300 to 350 μl.

Pulse sequences

The degree of protonation at the C^{α} position of individual amino acid types in the partially deuterated DFPase sample was probed as described by Rosen et al. (1996), using a 2D [^{15}N, ^{1}H]-TROSY version of a HN(CO)(CA) sequence. Briefly, two spectra were acquired which included a fixed period of transverse $^{13}C^{\alpha}$ magnetization adjusted to $1/(2^{1}J_{CH})$. In the first one, the $^{1}H^{\alpha}$-$^{13}C^{\alpha}$ scalar coupling is refocused (reference experiment), whereas in the second one the coupling is allowed to evolve such that magnetization of protonated $^{13}C^{\alpha}$ nuclei is dephased and cannot be converted into detectable magnetization in the remainder of the sequence (attenuated experiment). Thus only amino acids which are deuterated at the C^{α} position contribute to the signal in the second experiment and the $i + 1$ cross peak intensity ratio I_{att}/I_{ref} is a measure of the deuteration level at C^{α} of residue i. In order to improve spectral resolution a semi-constant time (Logan et al., 1992; Grzesiek and Bax, 1993a) ^{15}N evolution period was employed.

Decay rates of the slowly relaxing ^{15}N and ^{1}H doublet components were determined from series of [^{15}N, ^{1}H]-TROSY experiments including spin-echo periods Δ of variable lengths (Boisbouvier et al., 1999; Kontaxis et al., 2000). For ^{15}N linewidth measurements, the $\Delta/2$-180°(^{15}N)-$\Delta/2$ period preceded the evolution period of a standard [^{15}N, ^{1}H]-TROSY sequence. Amide proton linewidths were measured with a $\Delta/2$-180°(^{1}H)-$\Delta/2$ period inserted prior to the acquisition priod. The 180°(^{1}H) pulse was a 1.5-ms RE-BURP (Geen and Freeman, 1991) pulse applied at 9.7 ppm and flanked by a pair of pulsed field gradients. This provides band-selective refocussing of the majority of amide protons while leaving the magnetization of the water and of α-protons untouched, thus decoupling scalar interactions during the spin-echo period. Each of the experiments was recorded in a 3D manner with Δ values incremented by a constant amount, such that linewidths could be directly extracted after Fourier transformation along the 'spin-echo dimension' at the ^{1}H and ^{15}N peak positions of individual residues in the regular TROSY frequency domains (Heikkinen and Kilpeläinen, 2001).

All H^{N}-based 'out-and-back' type triple-resonance experiments employed to obtain sequential assignments were recorded as [^{15}N, ^{1}H]-TROSY versions (Pervushin et al., 1997; Salzmann et al., 1998, 1999a), using a gradient echo/antiecho coherence selected, sensitivity enhanced detection scheme (Czisch and Boelens, 1998; Pervushin et al., 1998; Weigelt, 1998) where the number of ^{1}H 180° pulses was minimized (Dingley and Grzesiek, 1998). The first part of the single transition-to-single transition polarization transfer (ST2-PT) period was concatenated with the respective $^{13}C \rightarrow {}^{15}N$ back transfer delay of the individual experiments as described previously (Loria et al., 1999; Salzmann et al., 1999b) in order reduce relaxation losses. During ^{1}H acquisition carbon spins were decoupled using a sequence of 3-ms WURST-20 (Kupče and Freeman, 1995) pulses of 80 kHz sweep, resulting in purely absorptive lineshapes and enhanced sensitivity (Yang and Kay, 1999b). Deuterium decoupling was applied during periods involving transverse magnetization of aliphatic ^{13}C spins to eliminate the effect of the ^{2}H quadrupolar interaction (Grzesiek et al., 1993). In pulse sequences applied to the partially deuterated DFPase sample ^{1}H-^{13}C couplings were refocussed during ^{13}C evolution times using pairs of unselective ^{1}H 180° pulses to preserve the spin states of amide protons, as required for the TROSY-type selection of the slowly relaxing ^{15}N doublet component (Fiala et al., 2000; Löhr et al., 2000; Eletsky et al., 2001). In all sequences water-selective 2.1-ms Gaussian-shaped flip back pulses were employed to align the water magnetization along the +z axis after the initial INEPT (Morris and Freeman, 1979) period and before acquisition, avoiding the saturation of fast exchanging amide protons (Grzesiek and Bax, 1993b; Stonehouse et al., 1994; Matsuo et al., 1996).

In addition to the TROSY-type $^{1}H^{N}$-based approach a suite of triple-resonance pulse sequences was applied, where the magnetization transfer pathway begins at $^{1}H^{\alpha}$ and where $^{1}H^{\alpha}/^{13}C^{\alpha}$ multiplequantum (MQ) coherences are created to make the mutual dipolar interaction ineffective in relaxing these nuclei (Griffey and Redfield, 1987; Seip et al., 1992; Grzesiek et al., 1995; Swapna et al., 1997; Yamazaki et al., 1997; Kong et al., 1999). All pulse schemes use a standard sensitivity enhanced reverse INEPT element (Palmer III et al., 1991) in conjunction with gradient coherence selection (Kay et al., 1992), and either α- or amide protons are finally detected. The (HCA)CO(CA)NH experiment (Löhr et al., 1995a) was recorded in an improved MQ version essentially as described by Tessari et al. (1997), the main difference involving the implementation of the semi-constant time t_1 evolution period, allowing for prolonged ^{13}CO acquisition times. In a similar manner, intra- and interresidual α-proton to amide ^{1}H and ^{15}N correlations (Montelione and Wagner, 1990;

Kay et al., 1991; Boucher et al., 1992) were obtained using the MQ-H(CA)NH pulse sequence shown in Figure 2A. The experimental scheme is closely related to the CTSL-HCANH sequence (Larsson et al., 1999), substituting a $^1H^\alpha$ for a $^{13}C^\alpha$ evolution period. As in the latter pulse sequence, transverse relaxation rates during the relatively long delay needed for dephasing of $^{13}C^\alpha$ magnetization with respect to ^{15}N are diminished by preparation of $^1H^\alpha/^{13}C^\alpha$ MQ coherence, and the dephasing due to scalar ^1H-^1H couplings is prevented by selectively spin-locking $^1H^\alpha$ (Grzesiek and Bax, 1995). However, in the course of t_1 the duration of the spin-lock pulse is gradually shortened to allow $^1H^\alpha$ chemical shift evolution. Therefore the t_1 period is semi-constant time with respect to homonuclear J-couplings, while it is constant-time with respect to relaxation. The initial free precession period T_H is adjusted to approximately $1/^1J_{CH}$, such that the number of ^1H and ^{13}C 180° pulses could be minimized.

Figures 2B and 2C depict modified versions of the HCACO (Ikura et al., 1990; Powers et al., 1991) and HCACB (Yamazaki et al., 1997) experiments, respectively. The novel MQ-HCACO sequence combines the advantages of a HMQC-type (Bax et al., 1983; Bendall et al., 1983) $^{13}C^\alpha$-^{13}CO correlation to achieve an optimized coherence transfer function and favourable $^{13}C^\alpha$ relaxation properties afforded by $^1H^\alpha/^{13}C^\alpha$ multiple-quantum coherence. As described previously (Bazzo et al., 1995; Löhr and Rüterjans, 1995b), the HMQC module makes it possible to adjust both periods for $^{13}C^\alpha$-^{13}CO magnetization transfers ($T_C^a + T_C^b$ in the scheme of Figure 2B) to $1/(2^1J_{C\alpha,CO})$ while refocussing the passive $^{13}C^\alpha$-$^{13}C^\alpha$ coupling by fixing the overall duration of transverse $^{13}C^\alpha$ magnetization ($= 2(T_C^a + T_C^b + T_C^c) = 4T_C^a$) at $1/^1J_{C\alpha,C\beta}$. The ^1H spin-locked $^1H^\alpha/^{13}C^\alpha$ multiple-quantum coherence warrants a sufficiently slow decay of magnetization during the latter interval (Yamazaki et al., 1997; Xia et al., 2000). In the present implementation this period could be exploited almost entirely for constant-time chemical shift evolution, ensuring a high resolution in the $^{13}C^\alpha$ frequency domain. The resolution in the semi-constant time carbonyl dimension is however limited by the evolution of $^1J_{C\alpha,C\beta}$ couplings and ^{13}CO R_2 relaxation. The MQ-HCACB sequence employs an 'out-and-back' type CC-COSY transfer between adjacent aliphatic carbons and is optimized to obtain $^1H^\alpha$-$^{13}C^\alpha$-$^{13}C^\beta$ connectivities. The $^1H^\alpha/^{13}C^\alpha$ multiple-quantum periods for de- and rephasing of α-carbon magnetization with respect to $^{13}C^\beta$ are tuned to $1/(2^1J_{C\alpha,C\beta})$. The second one is used for constant-time $^{13}C^\alpha$ chemical shift labelling as a function of t_2. As in the HCACO a selective $^1H^\alpha$ spin-lock suppresses proton-proton scalar couplings and chemical shift evolution during these periods. Since β-carbons may be attached to either protons or deuterons in the partially deuterated protein sample, both ^2H composite pulse decoupling and a ^1H refocussing pulse are applied during the $^{13}C^\alpha$ evolution time t_1. Further details of the MQ-HCACO and MQ-HCACB pulse sequences are given in the Figure legend.

Both MQ-HCACO and MQ-HCACB pulse sequences employ a gradient-sensitivity enhancement element (Kay et al., 1992) to transfer magnetization back for $^1H^\alpha$ detection. For very large proteins this scheme may actually lead to reduced sensitivity because of fast relaxation during the addional $1/(2^1J_{CH})$ period and additional RF pulses. In the case of DFPase, increased sensitivity was observed as verified by comparing 2D ^1H,^{13}C-HSQC spectra recorded with and without sensitivity enhancement. Furthermore, it should be noted that the variable ^1H spin-lock periods in MQ-H(CA)NH and MQ-HCACO experiments may introduce t_1-noise due to temperature effects. However, since the required RF power levels are moderate and the variation is limited to only 10–15 ms, this effect is small. In fact, no such problems were encountered in the spectra of DFPase.

Side-chain carbon to amide $^{15}N/^1H$ connectivities were obtained using the C(CC)(CO)NH pulse sequence (Farmer II and Venters, 1995). Its magnetization transfer pathway starts with ^{13}C polarization and no attempt was made to utilize proton polarization via an initial INEPT step for the protonated side-chain carbon sites in the partially deuterated protein. However, by saturating protons during the relaxation delay, the heteronuclear NOE was exploited to obtain signal enhancement. Isotropic mixing was achieved with the FLOPSY-8 sequence (Mohebbi and Shaka, 1991), applied with an RF field strength of 8.3 kHz for a duration of 17 ms.

Data acquisition and processing

Spectra were recorded on either 600- or 800-MHz four-channel Bruker Avance spectrometers equipped with 5 mm $^1H\{^{13}C/^{15}N\}$ three-axis gradient triple-resonance probes. The temperature was adjusted to 28 °C in all experiments.

The [^{15}N, ^{1}H]-TROSY-HN(CO)(CA) experiment for determination of the C^{α} deuteration level of partially labelled DFPase was carried out at 600 MHz ^{1}H Larmor frequency. Attenuated and reference spectra were recorded in an interleaved manner using spectral widths of 34.3 and 13.6 ppm along the ^{15}N (ω_1) and ^{1}H (ω_2) dimensions, with the carrier position centered at 119 and 4.75 ppm (H_2O) respectively. Time domain data consisted of 160 × 768 complex points, corresponding to acquisition times of 76.8 ms in t_1 and 94 ms in t_2. A recycle delay of 7 s was employed to ensure restoration of amide proton equilibrium magnetization between transients, irrespective of differential R_1 relaxation rates of C^{α} protonated and deuterated amino acids. Accumulation of 32 scans per FID resulted in a total measurement time of 41 h.

Linewidths of the slowly relaxing (TROSY) ^{1}H and ^{15}N doublet components were measured at 800 MHz for fully protonated (and ^{15}N-labelled), partially deuterated (and ^{13}C/^{15}N-labelled) and fully deuterated (and ^{13}C/^{15}N-labelled) DFPase. For the latter two samples ^{1}H spin-echo periods Δ were incremented from 1.6 to 151.6 ms in intervals of 10 ms, whereas for the ^{15}N labelled protein the longest value was 91.6 ms. The Δ interval for the determination of ^{15}N linewidths was 16 ms with a maximum duration of 241.6 ms. In all experiments spectral widths in the ^{15}N and ^{1}H dimensions were 40 and 16.9 ppm, respectively, and 200 (t_1) × 1024 (t_2) complex points were recorded, resulting in acquisition times of 61.3 and 75.6 ms. Four scans were recorded per FID, except for the ^{1}H linewidths determination in ^{15}N-labelled DFPase, where eight scans were accumulated, giving rise to measurement times of approximately 20 h for each of the three-dimensional data sets.

Relevant acquisition parameters of all 3D triple-resonance experiments for resonance assignments applied to the partially deuterated, ^{13}C/^{15}N-labelled sample are summarized in Table 1. The variables λ (MQ-H(CA)NH) and χ (MQ-HCACO) were adjusted to 0.92 and 0.5, respectively.

Processing and spectra analysis was carried out using the NMRPipe/NMRDraw (Delaglio et al., 1995) software. The residual water signal was eliminated by time-domain convolution in the directly detected dimensions (Marion et al., 1989a). Linear prediction was applied in indirectly detected dimensions to extend time-domain data by $\frac{1}{4}$ to $\frac{1}{3}$ of their original length. Prior to Fourier transformation, data were multiplied with squared-cosine weighting functions in all dimensions. Linear prediction and apodization were not applied in the linewidth dimensions of the 3D linewidth-resolved [^{15}N, ^{1}H]-TROSY spectra. Here, digital resolutions after zero-filling and Fourier transformation along the respective ^{1}H and ^{15}N spin-echo dimensions were 0.78 and 0.49 Hz pt^{-1}. Linewidths were extracted by fitting Lorentzian lines using NMRLAB (Günther et al., 2000).

Results and discussion

Obtaining resonance assignments of ^{13}C/^{15}N-labelled proteins in the 300-residue range is severely impeded by fast R_2 relaxation which makes most triple-resonance pulse sequences ineffective and aggravates signal overlap. Perdeuteration, commonly employed as a remedy to reduce dipolar relaxation, must however be followed by complete back-exchange of amide protons. As previously reported (McCallum et al., 1999; Wang et al., 1999; Riek et al., 2002; Tugarinov et al., 2002), very slow back-exchange in larger proteins renders significant fractions of signals undetectable, unless the proteins can be denatured and refolded *in vitro*. For the same reason, application of a suite of HN-based [^{15}N, ^{1}H]-TROSY type triple-resonance experiments (Salzmann et al., 1998, 1999a, c; Loria et al., 1999; Löhr et al., 2000) to fully ^{2}H/^{13}C/^{15}N enriched DFPase resulted in fragmentary and ambiguous sequential assignments (data not shown). Therefore it was investigated whether a partially deuterated sample, produced by growing bacteria on fully deuterated algal lysate in H_2O meets the requirements to completely assign main chain resonances of a larger protein featuring numerous practically unexchangeable amide hydrogens. This approach yields protein molecules that are fully protonated at all amide sites as opposed to fractionally deuterated samples expressed in D_2O-based minimal media containing a non-deuterated carbon source.

Assuming identical yields the proposed labelling scheme is more expensive than perdeuteration using minimal medium in D_2O. However, when the perdeuterated protein must be expressed from deuterated algal lysate medium in D_2O, the cost of our labelling scheme is lower because H_2O is used.

Characterization of $^{1}H^{\alpha}/^{2}H/^{13}C/^{15}N$-labelled DFPase

Some features of a partially ^{2}H enriched sample prepared from the H_2O-based deuterated algal lysate medium can already be observed in its one-

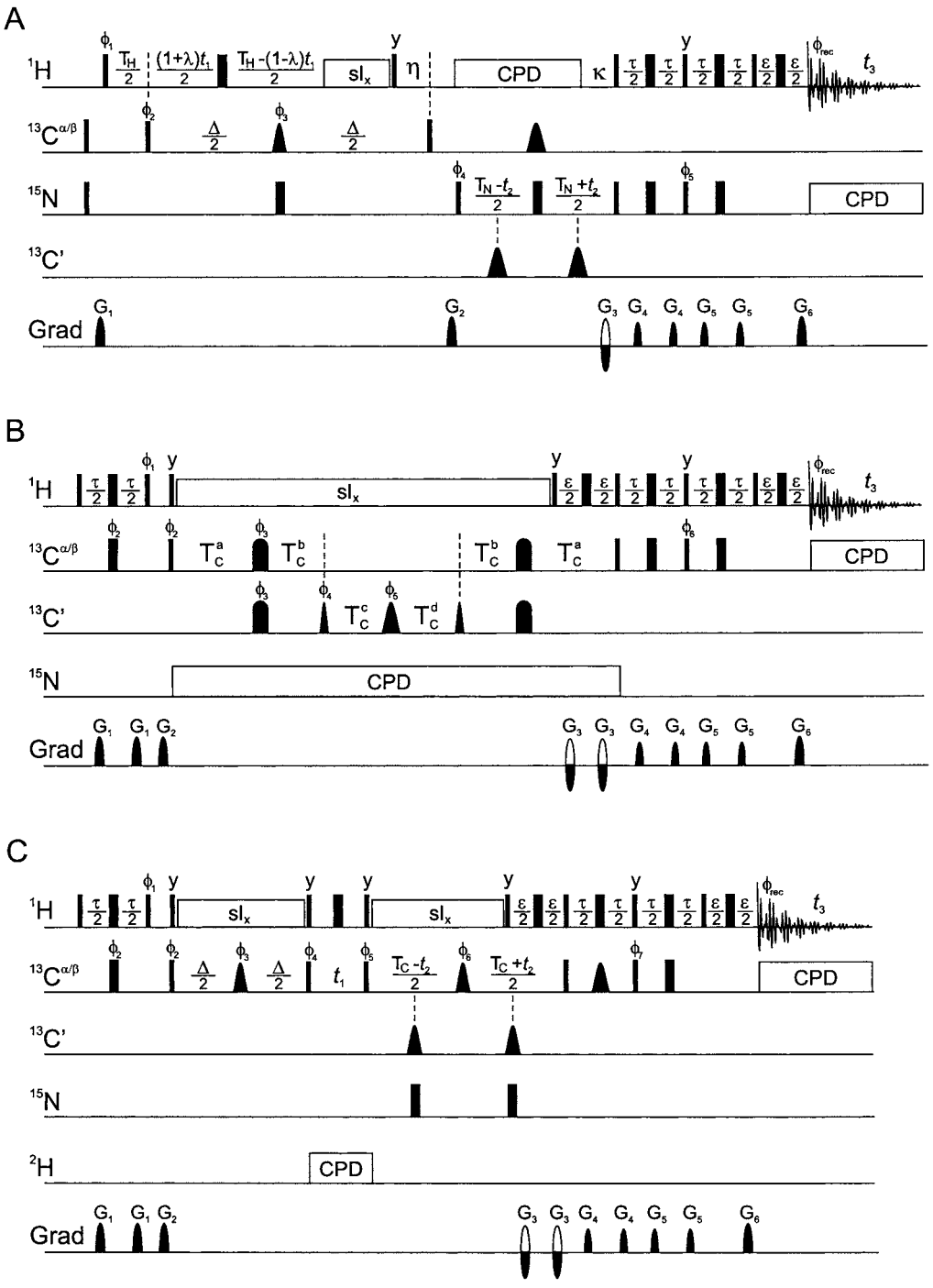
A
B
C
CPD
Grad

Table 1. Acquisition parameters for 3D experiments applied to obtain resonance assignments of uniformly $^{13}C/^{15}N$, partially ^{2}H-labelled DFPase

Experiment	Detected nucleus			Time domain data[a]			Spectral widths			Acquisition times			No. of scans per FID	Total exp. time (h)
	F_1	F_2	F_3	t_1	t_2	t_3	F_1 (ppm)	F_2 (ppm)	F_3 (ppm)	t_1 (ms)	t_2 (ms)	t_3 (ms)		
TROSY-HNCO[b]	^{13}CO	^{15}N	$^{1}H^{N}$	38	48	512	12.2	30.0	13.6	20.7	26.3	62.7	4	21
TROSY-HN(CA)CO[b]	^{13}CO	^{15}N	$^{1}H^{N}$	33	48	512	12.7	30.0	13.6	17.2	26.3	62.7	16	69
TROSY-HNCACB[c]	$^{13}C^{\alpha/\beta}$	^{15}N	$^{1}H^{N}$	86	44	768	55.8	20.0	13.6	7.7	27.1	70.7	8	67
(HCA)CO(CA)NH[b]	^{13}CO	^{15}N	$^{1}H^{N}$	38	48	512	12.2	30.0	13.6	20.7	26.3	62.7	32	88
H(CA)NH[c]	$^{1}H^{\alpha}$	^{15}N	$^{1}H^{N}$	52	64	640	4.0	30.0	13.6	16.2	26.4	58.8	16	84
HCACO[b]	^{13}CO	$^{13}C^{\alpha}$	$^{1}H^{\alpha}$	42	88	384	15.0	24.0	8.5	18.5	24.3	75.6	16	66
HCACB[b]	$^{13}C^{\beta}$	$^{13}C^{\alpha}$	$^{1}H^{\alpha}$	60	96	256	62.5	48.0	6.5	6.4	13.2	65.8	16	92
C(CC)(CO)NH[b]	^{13}C	^{15}N	$^{1}H^{N}$	64	48	384	63.1	20.0	10.5	6.7	39.4	60.9	16	140

[a]Complex points.

[b]Recorded at 600 MHz.

[c]Recorded at 800 MHz.

Figure 2. MQ versions of (A) H(CA)NH, (B) HCACO and (C) HCACB experiments, described for applications at 800 MHz (A) and 600 MHz (B and C) ^{1}H frequency. Narrow and wide filled bars denote rectangular 90° and 180° pulses applied along the x-axis unless indicated otherwise. Proton, deuterium and nitrogen carrier frequencies are centered at the water resonance (4.75 ppm), in the aliphatic region (3 ppm) and in the backbone amide region (118 ppm), respectively. In the H(CA)NH experiment, the ^{1}H carrier is temporarily switched to 8.5 ppm for amide proton composite pulse decoupling (CPD), which is performed with a DIPSI-2 (Shaka et al., 1988) sequence applied at an RF field of 5 kHz. Carrier frequencies of the ^{13}C channels are positioned at 56 ppm (sequence A), 54.2 ppm (B) and 44 ppm (C). Composite pulse decoupling of ^{13}C and ^{15}N spins is accomplished by GARP-1 modulations (Shaka et al., 1985), applied with RF field strengths of 1.7 kHz and 1.0 kHz, respectively. Deuterium decoupling employs a 0.8 kHz WALTZ-16 sequence (Shaka et al., 1983). 'sl' denotes a cw spin-lock with an RF field of 4 kHz (3.4 kHz) at 800 MHz (600 MHz) proton frequency. In sequence A, its initial duration of $\Delta - \eta - T_H/2$ is decremented by λt_1 in the course of the ^{1}H evolution time to retain a constant period of transverse ^{1}H and ^{13}C magnetization, in sequence B the duration of the the spin-lock period is incremented as a function of t_1 (see below), whereas in sequence C spin-lock periods are fixed. Rectangular carbon pulses are applied with 18.5 kHz (15.6 kHz) RF field strengths at 800 MHz (600 MHz) spectrometers. The shaped 180° ^{13}C pulses in the Δ and T_N periods of sequence A are G^3 Gaussian cascades (Emsley and Bodenhausen, 1990) with durations of 200 and 300 μs, respectively, where the first one is applied at 44 ppm using phase modulation of the RF (Boyd and Soffe, 1989; Patt, 1992). Sinc-shaped carbonyl 180° pulses are applied at 176 ppm and have a duration of 100 μs. In sequence B, sinc-shaped 90° and 180° pulses on carbonyls have a duration of 124 μs and a cosine-modulated amplitude profile to provide two excitation maxima at ± 122 ppm from the ^{13}C carrier position, thus avoiding non-resonant phase shifts on α-carbons (McCoy and Mueller, 1992). Simultaneous refocussing of $^{13}C^{\alpha/\beta}$ magnetization and inversion of $^{13}C'$ magnetization between periods T_C^a and T_C^b is achieved with a single 500-μs WURST-20 (Kupče and Freeman, 1995) pulse (80 kHz sweep), centered at 100 ppm. Sequence C employs 250 μs G^3 shaped 180° $^{13}C^{\alpha/\beta}$ pulses except for the G^3 pulse in the midpoint of the second τ period, which has a duration of 900 μs and is applied at 58 ppm through phase modulation to selectively invert α-carbon magnetization. Fixed delays are adjusted to (A) $T_H = 6.1$ ms, $\Delta = 26$ ms, $\eta = 3$ ms, $T_N = 24$ ms, $\kappa = 5.4$ ms, $\tau = 4.6$ ms and $\varepsilon = 0.8$ ms, (B) $\tau = 3.2$ ms and $\varepsilon = 0.8$ ms, (C) $\tau = 3$ ms, $\Delta = T_C = 13.2$ ms, $\varepsilon = 0.8$ ms. Initial durations of ^{13}C evolution periods ($t_1 = t_2 = 0$) in sequence B are $T_C^a = 6.97$ ms, $T_C^c = T_C^d = 4.53$ ms and $T_C^b = T_C^a - T_C^c - \tau(90° C') - \tau(180° C')/2$, where $\tau(90° C')$ and $\tau(180° C')/2$ are the widths of 90° and 180° carbonyl pulses. Carbonyl chemical shifts evolve in a semi-constant time manner by incrementing T_C^c by $(1 + \chi)t_1/2$ and decrementing T_C^d by $(1 - \chi)t_1/2$, where the factor χ is defined as $1 - 2T_C^d/t_{1\,max}$. Constant time $^{13}C^{\alpha}$ chemical shift evolution occurs in t_2 by shifting the two WURST-20 pulses towards the flanking rectangular 90° $^{13}C^{\alpha}$ pulses. In addition, periods T_C^a and T_C^b are altered in the opposite direction as a function of t_1 to avoid a modulation due to $^{13}C^{\alpha}$ chemical shifts in the $^{13}C'$ domain, yielding $T_C^a = T_C^a(t_1 = t_2 = 0) - (t_2 - \chi t_1)/4$ and $T_C^b = T_C^b(t_1 = t - 2 = 0) + (t_2 - \chi t_1)/4$ with $t_{2\,max} = 4(T_C^a - \varepsilon)$. Pulsed field gradients are sine-bell shaped and have the following durations, peak amplitudes and directions: (A) G_1, 0.5 ms, 10 G cm^{-1}, z; G_2, 0.5 ms, 25 G cm^{-1}, z; G_3, 1.6 ms, −19.23 G cm^{-1}, z; G_4, 0.3 ms, 4 G cm^{-1}, z; G_5, 0.3 ms, 5.5 G cm^{-1}, z; G_6, 0.2 ms, 16 G cm^{-1}, z; (B) G_1, 0.5 ms, 5 G cm^{-1}, x; G_2, 0.5 ms, 5 G cm^{-1}, y; G_3, 0.2 ms, −39.77 G cm^{-1}, xyz; G_4, 0.3 ms, 4 G cm^{-1}, xy; G_5, 0.3 ms, 5.5 G cm^{-1}, xy; G_6, 0.2 ms, 20 G cm^{-1}, xyz; (C) G_1, 0.6 ms, 5 G cm^{-1}, x; G_2, 0.6 ms, 5 G cm^{-1}, y; G_3, 0.2 ms, −48.72 G cm^{-1}, xyz; G_4, 0.5 ms, 4 G cm^{-1}, xy; G_5, 0.5 ms, 5.5 G cm^{-1}, xy; G_6, 0.2 ms, 24.5 G cm^{-1}, xyz. Phases are cycled according to: (A) $\phi_1 = 2(x), 2(-x)$; $\phi_2 = x, -x$; $\phi_3 = 4(x), 4(-x), 4(y), 4(-y)$; $\phi_4 = 4(x), 4(-x)$; $\phi_5 = y$; $\phi_{rec} = R, 2(-R), R$; (B) $\phi_1 = y, -y$; $\phi_2 = 4(x), 4(-x)$; $\phi_3 = 8(x), 8(-x)$, $\phi_4 = 2(x), 2(-x)$; $\phi_5 = 4(x), 4(-x), 4(y), 4(-y)$; $\phi_6 = y$; $\phi_{rec} = R, 2(-R), R$; (C) $\phi_1 = y, -y$; $\phi_2 = 2(x), 2(-x)$; $\phi_3 = 8(x), 8(y)$, $\phi_4 = y, -y$; $\phi_5 = 8(y), 8(-y)$; $\phi_6 = 4(x), 4(y)$; $\phi_7 = y$; $\phi_{rec} = R, 2(-R), R$, where R = x, 2(−x), x. Echo- and antiecho coherence transfer pathways are selected alternately by inverting the polarity of G_3 together with pulse phases (A) ϕ_5, (B) ϕ_6 and (C) ϕ_7. Axial peaks are shifted to the edge of the spectrum in sequences (A) and (B) by inverting ϕ_4 and ϕ_2, respectively, and the receiver phase in every other t_2 increment. Sign discrimination in the F_1 dimensions is accomplished by States-TPPI (Marion et al., 1989b) applied to phases (A) ϕ_1, (B) ϕ_4, (C) ϕ_2, ϕ_3 and ϕ_4.

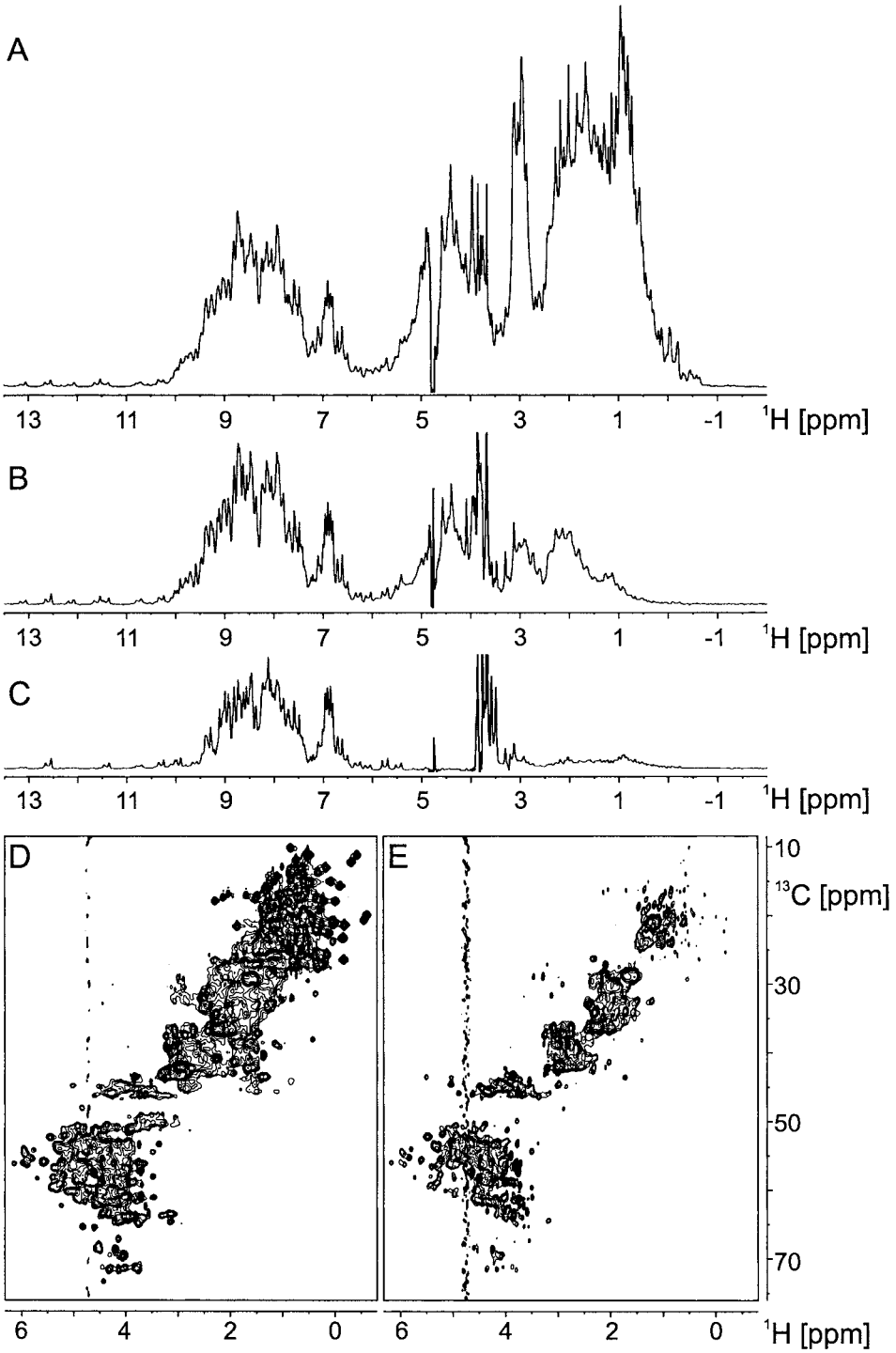

Figure 3. ^{1}H spectra of (A) 1.6 mM ^{13}C/^{15}N-, (B) 0.6 mM ^{1}H$^{\alpha}$/^{2}H/^{13}C/^{15}N- and (C) 0.9 mM ^{2}H/^{13}C/^{15}N-labelled DFPase and aliphatic portions of ^{1}H,^{13}C-HSQC spectra of (D) 1.6 mM ^{13}C/^{15}N- and (E) 0.6 mM ^{1}H$^{\alpha}$/^{2}H/^{13}C/^{15}N-labelled DFPase. All samples were dissolved in 10 mM Bis-Tris-propane buffer, pH = 6.5, containing 5% D_2O. One-dimensional spectra were recorded at 800 MHz using a simultaneous ^{13}C and ^{15}N heteronuclear spin-echo difference pulse sequence to suppress the otherwise very strong buffer signal at $\approx$3.8 ppm. No decoupling was applied during acquisition. The water signal was suppressed by presaturation. Different number of scans were acquired to account for the variation in protein concentrations. Spectra are vertically scaled to obtain an approximately equal noise level. Two dimensional HSQC spectra were recorded at 600 MHz employing gradient coherence selection and sensitivity enhancement (Kay et al., 1992). Eight and 32 scans, respectively, were accumulated for each FID in the experiments presented in D and E.

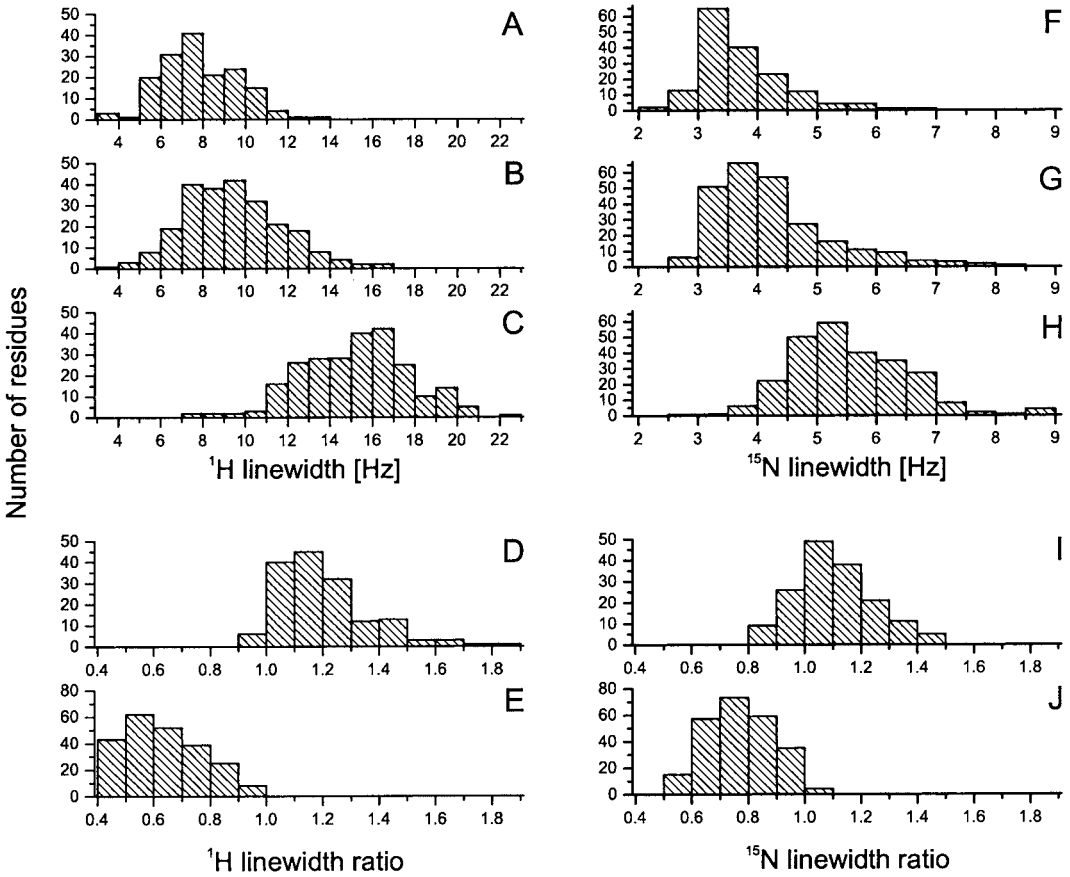

Figure 4. Histograms showing the distribution of ^{1}H (left column) and ^{15}N (right column) linewidths (full widths at half-height, $\Delta\nu_{1/2}$) determined from 3D linewidth-resolved [^{15}N, ^{1}H]-TROSY spectra of (A, F) ^{2}H/^{13}C/^{15}N-, (B, G) ^{1}H$^\alpha$/^{2}H/^{13}C/^{15}N- and (C, H) ^{15}N-labelled DFPase. In the lower two panels linewidth ratios are given between (D, I) ^{1}H$^\alpha$/^{2}H/^{13}C/^{15}N- and ^{2}H/^{13}C/^{15}N- and between (E, J) ^{1}H$^\alpha$/^{2}H/^{13}C/^{15}N- and ^{15}N-labelled protein.

dimensional proton NMR spectrum. Figures 3A–C compare ^{1}H spectra of partially deuterated DFPase with those of non-deuterated DFPase resulting from bacterial growth in minimal medium containing fully protonated carbon sources and of perdeuterated DFPase prepared from a deuterated algal lysate in D_2O, supplemented with deuterated glucose. It is apparent (i) that linewidths of amide resonances gradually decrease with increasing deuteration levels, (ii) that the number of signals in the region downfield from 8.5 ppm, containing only signals from amide and tryptophan N$^{\varepsilon 1}$-protons, is very similar in the non-deuterated and partially deuterated species but significantly lower in perdeuterated DFPase as a consequence of incomplete proton back-exchange. It can also be seen that (iii) the overall signal intensity in the methyl region of partially deuterated DFPase is considerably reduced when compared with the non-deuterated protein whereas differences in the α-proton region are smaller. The ^{1}H incorporation can be studied in a more detailed but still qualitative manner from two-dimensional ^{1}H-^{13}C correlation maps. The aliphatic regions from HSQC (Bodenhausen and Ruben, 1980) spectra of non-deuterated and partially deuterated DFPase are shown in Figures 3D and 3E, respectively. Most of the ^{1}H$^\alpha$-^{13}C$^\alpha$ correlations can still be observed in the partially deuterated sample, but many side-chain signals, especially those of methyl groups, show reduced intensities or are even absent. Compared to the spectrum of the fully protonated protein, the remaining signals are sharper in the proton dimension. This can be attributed to the lower proton density and the concomitantly reduced R_2 relaxation rates and scalar couplings. With respect to its deuteration pattern this DFPase sample is complementary to fractionally ^{2}H-labelled proteins, produced by grow-

ing bacteria in media containing a protonated carbon source in D_2O because the latter exhibits higher degrees of protonation in the side-chain positions than at C^{α}. Henceforth the partially deuterated protein sample used in this study is designated as $^{1}H^{\alpha}/^{2}H/^{13}C/^{15}N$-labelled in analogy to Yamazaki et al. (1997), although it should be noted that the preference for C^{α} protonation versus side-chain protonation in this sample is less pronounced than in proteins expressed in growth media containing selectively $^{1}H^{\alpha}$- and uniformly $^{2}H/^{13}C/^{15}N$-labelled amino acids as proposed by Yamazaki and co-workers.

Using the NMR method described by Rosen et al. (1996) the level of proton incorporation at C^{α} from water in the growth medium was quantitatively analysed on a residue-type specific basis. The experiment relies on the dephasing of $^{13}C^{\alpha}$ magnetization by the $^{1}J_{C\alpha H\alpha}$ interaction in amino acids protonated at this position, leading to a loss of signal intensity relative to an experiment recorded with refocussing of the scalar coupling evolution, which is proportional to the fractional protonation level. Signal intensities are monitored in 2D spectra at the $^{1}H/^{15}N$ resonance positions of sequentially following residues using a HN(CO)CA type pulse sequence. Results obtained for all 20 amino acid types are listed in Table 2. It should be noted that intensity ratios in protonated and deuterated amino acids are affected by the different $^{13}C^{\alpha}$ transverse relaxation rates during the J evolution delay. Assuming T_2 times of 10 ms and 60 ms for the protonated and deuterated species, respectively, the values in Table 2 which are not corrected for this effect, overestimate the deuteration levels by up to 7%. Data obtained for DFPase reveal a wide distribution of ^{1}H incorporation during bacterial growth in a medium containing fully deuterated algal lysate, depending on the amino acid type. While amino acids such as proline, arginine and histidine remain almost completely deuterated, very high C^{α} protonation levels are obtained for tryptophan, asparagine and aspartate. Thus it can be anticipated that, for the first group, H^{N}-based 'out-and-back' type triple-resonance pulse sequences that include long periods of transverse $^{13}C^{\alpha}$ magnetization will perform well, whereas they will severely suffer from fast R_2 relaxation rates of the protonated α-carbons for the latter residue types. Conversely, the efficiency of H^{α}-based experiments is proportional to the C^{α} protonation level making them most suitable for residues such as Trp, Asx or Gly, whereas they will obviously fail to provide cross peaks for Pro, Arg and His due to the lack of α-protons. Amino acids with intermediate protonation levels might give rise to useful correlations in both types of experiments.

To some extent the deuteration levels reported in Table 2 reflect the relative amounts of amino acids present in the algal lysate, because protons from H_2O are incorporated during bacterial biosynthesis when deuterated amino acids are depleted (Markus et al., 1994). Therefore some variation may be expected depending on the algal lysate. It is less likely, however, that the amino acid composition of a specific protein affects the C^{α} deuteration levels.

The efficiency of [^{15}N, ^{1}H]-TROSY type triple-resonance pulse sequences not only depends on R_2 rates of the correlated ^{13}C nuclei, but to a significant degree on relaxation properties of amide protons and nitrogens, too. To assess the impact of the different proton densities of non-deuterated, partially deuterated and perdeuterated protein samples, transverse relaxation rates of ^{1}H and ^{15}N TROSY doublet components were determined. In order to match the conditions relevant for relaxation during triple-resonance pulse schemes, the signal decay was measured using simple Hahn echo modules rather than CPMG (Carr and Purcell, 1954; Meiboom and Gill, 1958) or $R_{1\rho}$ (Deverell et al., 1970) techniques. Because the pulse sequence for the measurement of ^{1}H linewidths employed band-selective refocussing pulses the analysis was limited to amide protons resonating between $\approx$ 12.0 and 7.4 ppm while no such restriction was imposed on the measurement of ^{15}N linewidths. Figure 4 summarizes the results obtained for DFPase. Average proton linewidths measured for the fully deuterated, partially deuterated and non-deuterated protein were 7.9, 9.4 and 15.2 Hz, respectively, with distributions depicted in histograms A–C. As expected, for all residues which could be evaluated, signals in spectra of the partially deuterated sample are narrower than those of the non-deuterated sample but, with very few exceptions, broader than those of perdeuterated DFPase. However, varying local proton densities within partially deuterated protein molecules, which depend on amino acid types in the vicinity of the observed amide proton, result in relatively large variations, shown in histograms D and E. Ratios for individual amide protons in partially deuterated and fully or non-deuterated protein species cover a range from 0.93 to 1.86 (mean: 1.20) and 0.40 to 0.99 (mean: 0.63), respectively. Similar trends are apparent for ^{15}N linewidths, as can be seen in the right half of Figure 4. They span ranges of 2.2 to 6.7, 2.6 to 8.5 and 2.9 to 9.0 Hz in fully deuterated, partially deuterated and

Table 2. Fractional C^{α} deuteration levels of DFPase from *Loligo vulgaris* expressed in *E. coli* using ^{2}H-labelled algal lysate dissolved in $^{1}H_2O$

Amino acid type[a]	Pro (14)	Arg (5)	His (4)	Lys (14)	Ile (11)	Thr (12)	Leu (13)	Tyr (7)	Val (17)
Deuteration level[b] (%)	98.2 ± 4.2	97.1 ± 2.4	96.4 ± 2.1	94.2 ± 3.9	88.3 ± 5.3	83.5 ± 7.1	83.4 ± 6.6	79.3 ± 7.0	73.6 ± 6.5
Amino acid type[a]	Ala (12)	Ser (5)	Phe (13)	Met (4)	Glx[c] (30)	Cys (6)	Gly[d] (17)	Asx[c] (26)	Trp (4)
Deuteration level[b] (%)	73.1 ± 4.3	71.3 ± 7.4	58.9 ± 7.1	54.3 ± 9.1	49.9 ± 9.9	37.0 ± 8.3	27.1 ± 5.7	21.6 ± 6.1	18.9 ± 3.8

[a]Number of residues employed to calculate averages given in parenthesis.
[b]Average percentage deuteration (± standard deviations) determined from intensity ratios of cross peaks in a pair of 2D HN(CO)(CA) spectra with and without $^{1}J_{C\alpha H\alpha}$ dephasing. Values are not corrected for differential $^{13}C^{\alpha}$ T_2 times of protonated and deuterated carbons.
[c]No systematic differences were found between Glu and Gln and between Asp and Asn.
[d]For glycines the experiment measures the fraction of fully deuterated α-CH_2 groups.

non-deuterated DFPase, respectively (see histograms F-H for distributions), with averages of 3.7, 4.3 and 5.5 Hz. In individual residues, ^{15}N lineshapes of the $^{1}H^{\alpha}/^{2}H/^{13}C/^{15}N$-labelled protein are on average 1.11 times broader than those of the fully deuterated protein but only 0.77 times as broad as those in a non-deuterated sample. Histograms shown in sections I and J of Figure 4 reveal somewhat narrower distributions of ^{15}N linewidth ratios compared to those found for protons, falling in the range from 0.81 to 1.48 for partially vs. fully deuterated and from 0.51 to 1.07 for partially vs. non-deuterated DFPase. These results demonstrate that in the partially deuterated protein a significant improvement of ^{1}H and ^{15}N relaxation properties in TROSY-type experiments compared to the non-deuterated species is achieved, despite its relatively high degree of protonation at C^{α}, i.e., adjacent to the amide sites.

Application of ^{1}HN- and $^{1}H^{\alpha}$-based triple-resonance experiments

Obtaining main chain resonance assignments by triple-resonance NMR spectroscopy relies pre-dominantly on the identification of sequentially neighbouring amides by common correlations of $^{1}H^{N}$ and ^{15}N chemical shifts with those of other nuclei in the scalar coupling network, such as $^{13}C^{\alpha}$, $^{13}C^{\beta}$, $^{13}C'$ and possibly $^{1}H^{\alpha}$. With increasing number of amino acid residues and thus degenerate frequencies the availability of several independent pathways for such 'sequential walks' gains more and more importance. The success of the corresponding triple-resonance experiments strongly depends on the relaxation behaviour of the involved nucei. In this respect, α-carbons which are either detected themselves or employed as relay spins play a pivotal role. Considering the linewidth variations in $^{1}H^{\alpha}/^{2}H/^{13}C/^{15}N$-labelled protein samples caused by non-uniform C^{α} protonation it is important to prove that this labelling pattern is suitable for resonance assignment along the entire backbone of a 35-kDa protein such as DFPase. As a first example, it will be shown to what extent the 'carbonyl pathway' can provide sequential assignment information. Interresidual $^{1}H_i^{N}$-$^{15}N_i$-$^{13}C'_{i-1}$ connectivities are obtained in a sensitive manner from the HNCO experiment even for larger, non-deuterated proteins. Their intraresidual counterpart ($^{1}H_i^{N}$-$^{15}N_i$-$^{13}C'_i$) is, however, more demanding (Clubb et al., 1992). The [^{15}N,^{1}H]-TROSY-HN(CA)CO sequence (Loria et al., 1999) employed in this study contains a period of transverse $^{13}C^{\alpha}$ magnetization as long as 28 ms ($\approx 1/^{1}J_{C\alpha C\beta}$). This is acceptable for fully deuterated proteins, but renders the experiment highly susceptible to C^{α} protonation in partially deuterated samples due to efficient dipolar relaxation.

Slices from a HN(CA)CO experiment obtained with a $^{1}H^{\alpha}/^{2}H/^{13}C/^{15}N$-labelled sample are shown in Figure 5. For both parts of the sequence shown in part A, no assignments were obtained using perdeuterated DFPase, because the amide protons of residues 128 through 133 and 199 through 203 were undetectable due to very slow D/H-exchange. With few exceptions pairs of $^{13}C'$ cross peak between adjacent residues were observed throughout the sequence in the HN(CA)CO spectrum of $^{1}H^{\alpha}/^{2}H/^{13}C/^{15}N$-labelled DFPase. Intra- and interresidual correlations can normally be distinguished by comparing peak intensities. In the HN(CA)CO spectrum of $^{1}H^{\alpha}/^{2}H/^{13}C/^{15}N$-labelled DFPase intensities of some interresidual cross peaks are of equal or even higher intensity compared to intraresidual ones (e.g., W131/L130, W201/L200 and D204/Y203 in Figure 5A). This is a consequence of the residue-type dependent degree of C^{α} protona-

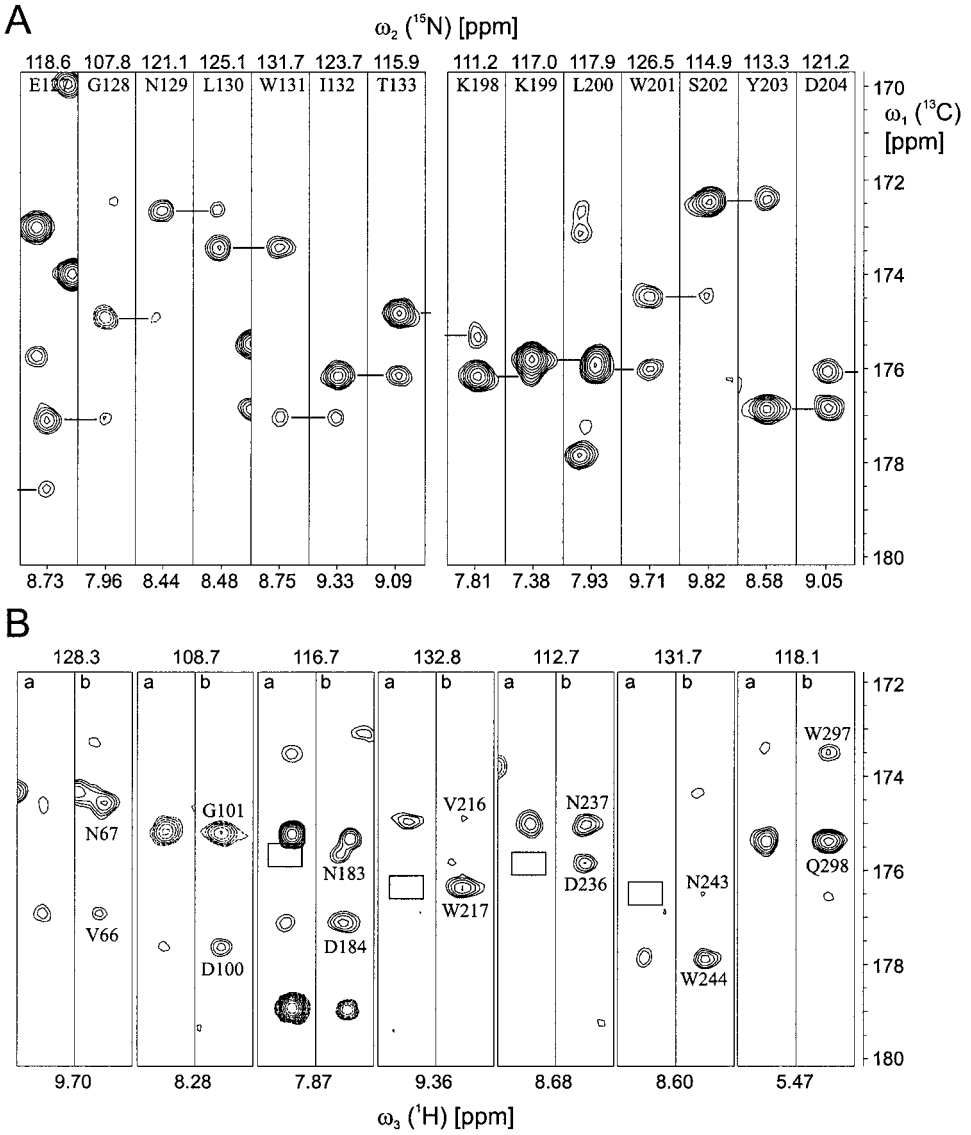

Figure 5. (A) Strip plot of a 3D [^{15}N,^{1}H]-TROSY-HN(CA)CO spectrum showing the sequential assignment of residues 127–133 and 198–204 of ^{1}H$^{\alpha}$/^{2}H/^{13}C/^{15}N-labelled DFPase. Connectivities are visualized by horizontal lines. The ^{13}C′ resonance frequencies of K198, K199 and L200 are almost degenerate, causing severe overlap in the ω_1 dimension. (B) Comparison of ^{13}C/^{1}H (ω_1/ω_3) strips taken from 3D [^{15}N,^{1}H]-TROSY-HN(CA)CO (left panels, a) and 3D (HCA)CO(CA)NH (right panels, b) spectra of ^{1}H$^{\alpha}$/^{2}H/^{13}C/^{15}N-labelled DFPase. In both experiments correlations involving glycine residues have a reversed sign due to the missing $\cos(\pi\Delta\,{}^{1}J_{C\alpha C\beta})$ dependence (Δ is a delay in the pulse sequences, adjusted to $1/{}^{1}J_{C\alpha C\beta}$). Assignments of intra- (residue i) and interresidual (residue $i-1$) cross peaks are drawn only in (HCA)CO(CA)NH strips. Empty boxes indicate missing peaks in the HN(CA)CO. Each strip has a width of 0.15 ppm along the ω_3 (^{1}H) dimension, centered around the chemical shift indicated at the bottom, and is taken at the ω_2 (^{15}N) resonance position shown on top of each slice. Solid and dashed contours represent positive and negative intensities, respectively, and are drawn on an exponential scale using a factor of $2^{1/2}$.

tion causing variable attenuation by transverse $^{13}C^{\alpha}$ relaxation during the ^{15}N-($^{13}C^{\alpha}$)-$^{13}C'$ relay step of the HN(CA)CO pulse sequence. Another possible reason for reversed relative intensities would be $^{2}J_{NC\alpha i-1} > {}^{1}J_{NC\alpha i}$, which can be excluded for our data (Wienk et al., 2003). Unequivocal identification of interresidual correlations was however warranted by recording an HNCO spectrum (data not shown).

In accordance with the C^{α} deuteration levels of DFPase (Table 2) Asn, Asp and Trp give rise to the lowest intensities in the HN(CA)CO spectrum. In some cases, signals were so weak that they could not be unambiguously identified or even absent. While missing interresidual correlations can easily be retrieved from the HNCO spectrum, a missing intraresidual correlation is absolutely detrimental for the sequential assignment process. For this reason a (HCA)CO(CA)NH experiment, which provides the same correlations as the HN(CA)CO (Löhr and Rüterjans, 1995a), was recorded in addition. In the used version (Tessari et al., 1997) the sequence takes advantage of $^{1}H^{\alpha}/^{13}C^{\alpha}$ multiple-quantum line-narrowing to slow down transverse $^{13}C^{\alpha}$ relaxation during the crucial $^{13}C^{\alpha} \rightarrow {}^{15}N$ coherence transfer step. Since the flow of magnetization in the (HCA)CO(CA)NH pulse sequence starts at $^{1}H^{\alpha}$, the resulting signal intensities are proportional to the C^{α} protonation level. In this sense the (HCA)CO(CA)NH experiment complements the HN(CA)CO in an ideal manner for $^{1}H^{\alpha}/^{2}H/^{13}C/^{15}N$-labelled proteins. Shown in Figure 5B are some examples where missing or very weak correlations involving Asn, Asp or Trp residues in the HN(CA)CO were readily observed in the (HCA)CO(CA)NH despite the lower overall sensitivity of the latter experiment, which does not employ TROSY-type signal enhancement. Note the absence of an intraresidual cross peak for Trp217 in the HN(CA)CO. As this residue exhibits very slow amide $^{2}H/^{1}H$ exchange preventing its detection in the spectra of perdeuterated DFPase, the (HCA)CO(CA)NH turned out to be essential for avoiding a break in the 'carbonyl pathway'.

Two additional independent pathways are provided by the HNCACB experiment (Wittekind and Mueller, 1993), which allows one to trace adjacent amide sites via common correlations with both α- and β-carbon nuclei. Owing to the shorter period of transverse $^{13}C^{\alpha}$ magnetization (≈ 14 ms) the pulse sequence is less susceptible to dipolar relaxation by directly attached protons than that of the HN(CA)CO resulting in more uniform signal intensities. Nevertheless, some amino acid type dependence is observed when applied to a $^{1}H^{\alpha}/^{2}H/^{13}C/^{15}N$-labelled proteins, calling for an additional experiment to unambiguously distinguish intra- from interresidual cross peak and, if necessary, detect interresidual connectivies missing in the HNCACB. For this purpose the HNCACB may be combined with CBCA(CO)NH (Grzesiek and Bax, 1992b) or HN(CO)CACB (Yamazaki et al., 1994) experiments. We preferred to record a C(CC)(CO)NH-TOCSY (Farmer II and Venters, 1995) spectrum, which yields the same type of information and additional side-chain carbon assignments beyond the C^{β} position. Because this sequence starts with carbon rather than proton polarization there is only a moderate dependence of cross peak intensities on protonation levels at individual side-chain positions, caused by relaxation and the $^{13}C\{^{1}H\}$-NOE exploited in the present application. Although this flow of magnetization results in a comparatively low overall sensitivity, in most cases the desired information could be readily extracted.

Figure 6 illustrates the combined use of HNCACB and C(CC)(CO)NH-TOCSY spectra of $^{1}H^{\alpha}/^{2}H/^{13}C/^{15}N$-labelled DFPase to assign amino acids Ile48 to Cys62 via the $^{13}C^{\alpha}/^{13}C^{\beta}$ pathway. Again, this fragment comprises several residues (i.e., Ile48-Ile51) that were not detectable in the perdeuterated protein. In most instances of the example shown, intraresidual correlations in the HNCAB are more intense than their interresidual counterparts. An exception is the Asp52/Ile51 link, where intraresidual cross peaks are weaker despite $^{1}J_{NC\alpha i} > {}^{2}J_{NC\alpha i-1}$ (Wienk et al., 2003). As described above, the reason for the change of intensities is the faster decay of transverse $^{13}C^{\alpha}$ magnetization in the aspartate residue due to its high degree of protonation. Unambiguous identification of intra- and interresidual connectivities is possible for these residues by the C(CC)(CO)NH-TOCSY, which contains only the latter. Some interresidual cross peaks with very low intensity in HNCACB (e.g., Gly56/Thr55 C^{α}, Lys57/Gly56 C^{α} and Cys62/Ile61 C^{α}/C^{β}) had higher sensitivity in the C(CC)(CO)NH-TOCSY. Moreover, the degeneracy of the Arg50/Leu49 $^{13}C^{\alpha}$ resonances giving rise to some ambiguity in the HNCACB was clearly established with the help of the C(CC)(CO)NH-TOCSY. Apart from $^{13}C^{\alpha}$ and $^{13}C^{\beta}$ the C(CC)(CO)NH-TOCSY spectrum provided many further side-chain carbon chemical shifts that allow more reliable identification of amino acid types and may be useful for subsequent structural studies.

While the preceding sections dealt with correlations which are in principle accessible to perdeuterated

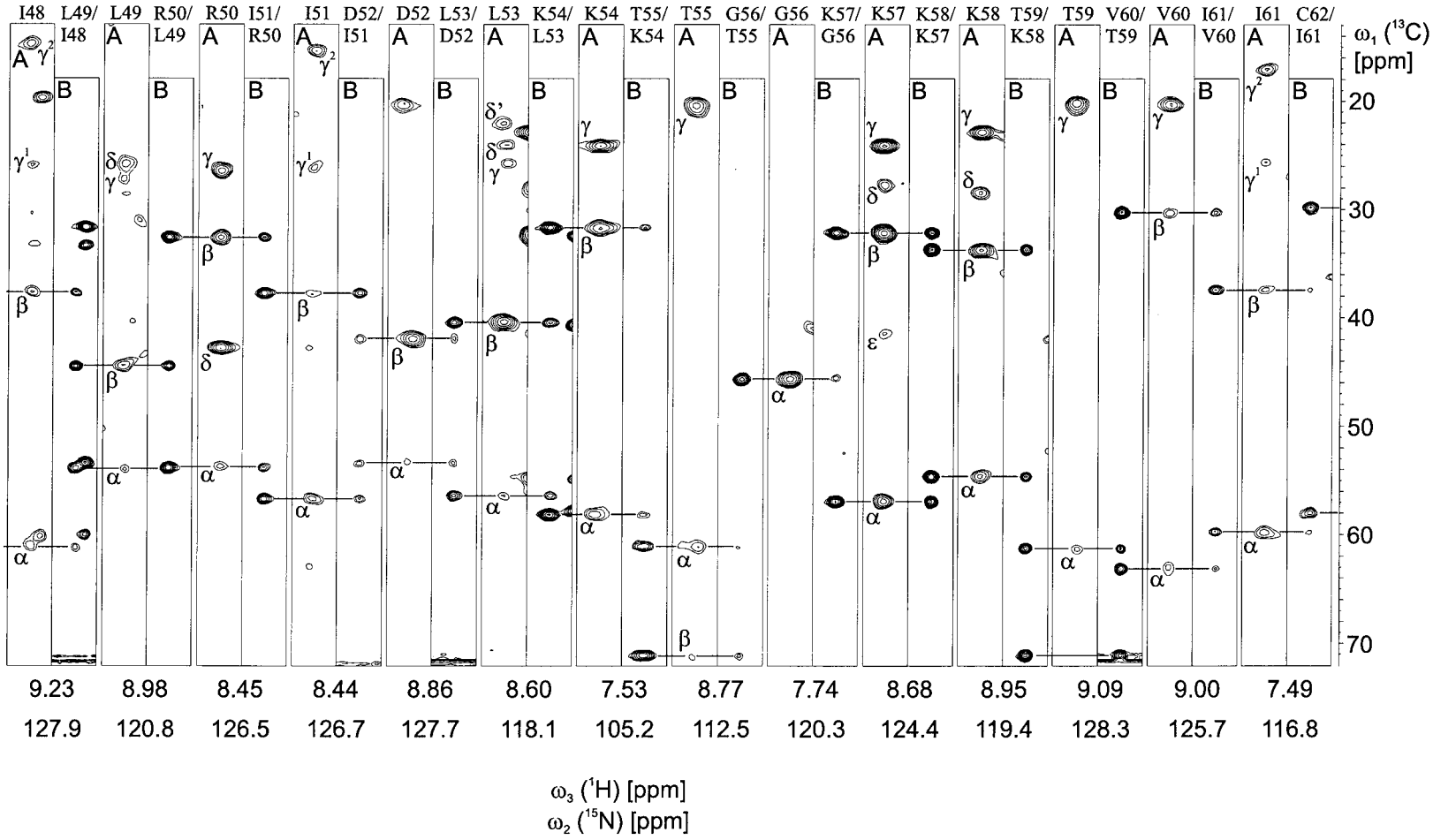

Figure 6. Backbone ^{15}N, ^{1}H and aliphatic ^{13}C resonance assignment for residues 48–62 of $^{1}H^{\alpha}/^{2}H/^{13}C/^{15}N$-labelled DFPase. The $^{13}C/^{1}H$ (ω_1/ω_3) sections are taken from (A) C(CC)(CO)NH-TOCSY and (B) [^{15}N,^{1}H]-TROSY-HNCACB spectra recorded at 600 and 800 MHz, respectively, and have a width of 0.15 ppm along ω_3. As indicated at the top, correlations involve ^{13}C chemical shifts of both residues i and $i-1$ in the [^{15}N,^{1}H]-TROSY-HNCACB, but exclusively those of residue $i-1$ in the C(CC)(CO)NH-TOCSY. Strips from both spectra are extracted at the ^{1}H and ^{15}N chemical shifts, given below each panel, of residue i. Positive and negative contours, spaced by a factor of $2^{1/2}$, are plotted without distinction. Horizontal lines connect intraresidual $^{13}C^{\alpha}$ and $^{13}C^{\beta}$ cross peaks in the HNCACB with the corresponding interresidual correlations of the sequentially following residue in both HNCACB and C(CC)(CO)NH-TOCSY. Assignments of α- and side-chain carbon resonances are indicated by greek letters in the C(CC)(CO)NH-TOCSY strips. Stereospecific assignments of leucine and valine methyl groups are not available.

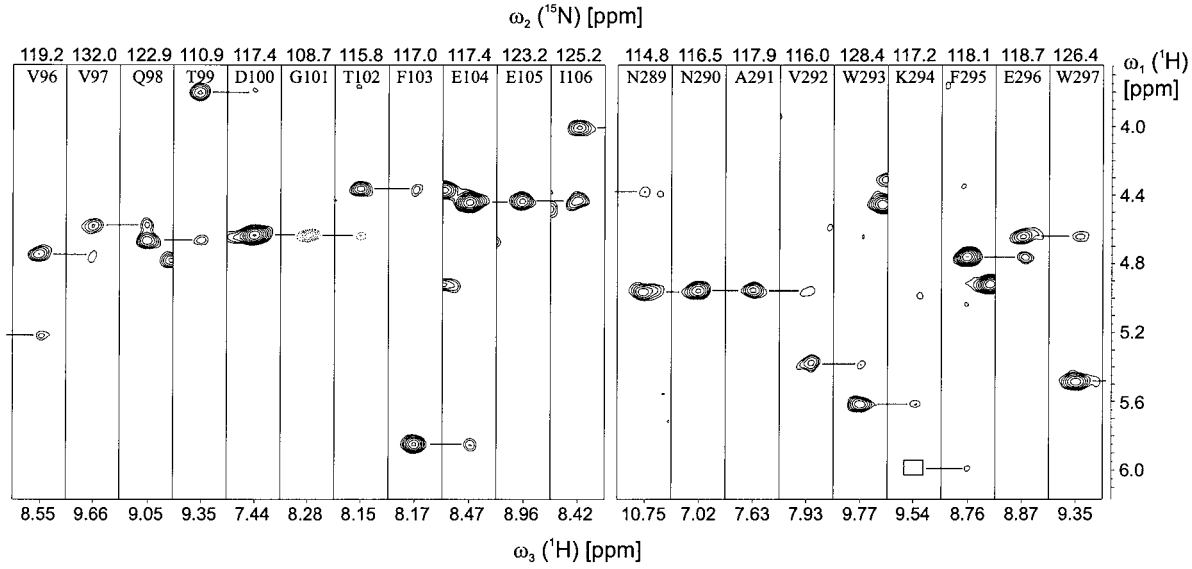

Figure 7. Strips from a 3D MQ-H(CA)NH spectrum showing the connectivities from two segments of DFPase. The regions from $^{1}H^{\alpha}/^{1}H^{N}$ (ω_1/ω_3) planes, taken at the ^{15}N (ω_2) chemical shifts and centered around the $^{1}H^{N}$ chemical shift indicated at the top and bottom, respectively, have a width of 0.15 ppm along ω_3. Positive and negative contours (level spacing factor $2^{1/2}$) are represented by solid and dashed lines, respectively. Straight horizontal lines mark sequential links via common $^{1}H^{\alpha}$ correlations. The intraresidual cross peak of Lys294 was not detected, as indicated by an empty box. Notice that the $^{1}H^{\alpha}$ resonance frequencies of sequential neighbours Asp100/Gly101, Glu104/Glu105 and Asn289/Asn290/Ala291 are degenerate.

molecules, the inclusion of α-protons in the resonance assignment of larger proteins, treated in the following, is quite unique for the $^{1}H^{\alpha}/^{2}H/^{13}C/^{15}N$-labelled species. Knowledge of $^{1}H^{\alpha}$ chemical shifts as such is of interest for evaluation of NOESY spectra and as an indicator of secondary structure. In addition, they are able to supplement the $^{13}C'$ and $^{13}C^{\alpha}/^{13}C^{\beta}$ pathways to find sequential links between backbone amide $^{1}H/^{15}N$ signals. A suitable pulse sequence for this purpose is the MQ-H(CA)NH, which correlates α-proton chemical shifts with those of amide protons and nitrogens of the same and the sequentially following residue via $^{1}J_{NC\alpha}$ and $^{2}J_{NC\alpha}$ couplings, respectively. An example is given in Figure 7, showing the sequential assignment of residues Val96 to Ile106 and Asn289 to Trp297 of DFPase, following the $^{1}H^{\alpha}$ pathway. Within these fragments, Val96, Val97, Ala291, Val292, Trp293, Lys294, Phe295 and Trp297 were among the residues exhibiting very slow amide exchange with the solvent. Therefore the use of the $^{1}H^{\alpha}/^{2}H/^{13}C/^{15}N$-labelled sample was essential to complete their assignment.

Figure 7 also reveals the major drawback of the methods employing $^{1}H^{\alpha}$ magnetization, the pronounced dependence of signal intensities on amino acid types. It should be mentioned that proline and arginine, which have the lowest protonation level at C^{α} (see Table 2), were not observed in the H(CA)NH spectrum and histidine and lysine signals are usually weak or absent. As a consequence, some of the extracted strips contain only a single rather than a pair of cross peaks, which may represent either the intraresidual or the sequential connectivity or just be a result of accidental $^{1}H^{\alpha}$ chemical shift degeneracy. Therefore, additional information is required to allow a distinction between the three cases. To this end MQ-HCACO and MQ-HCACB experiments were performed, both providing intraresidual correlations exclusively. Moreover, since the pulse sequences rely on large $^{1}J_{CH}$ and $^{1}J_{CC}$ couplings only, their inherent sensitivity is higher than that of the MQ-H(CA)NH, where the crucial polarization transfer step depends on comparatively small $^{13}C^{\alpha}$-^{15}N couplings. As an example, intraresidual correlations of Lys294, not detected in the MQ-H(CA)NH, were readily observed in MQ-HCACO and MQ-HCACB experiments (not shown). Figure 8 demonstrates their use to lift $^{1}H^{\alpha}$ degeneracies of sequential neighbours which gave rise to ambiguities in the MQ-H(CA)NH. For instance, the ω_1/ω_2 planes at $\omega_3 = 4.45$ ppm contain three pairs of sequential neighbours, which appear as well separated signals, whereas only a single correlation

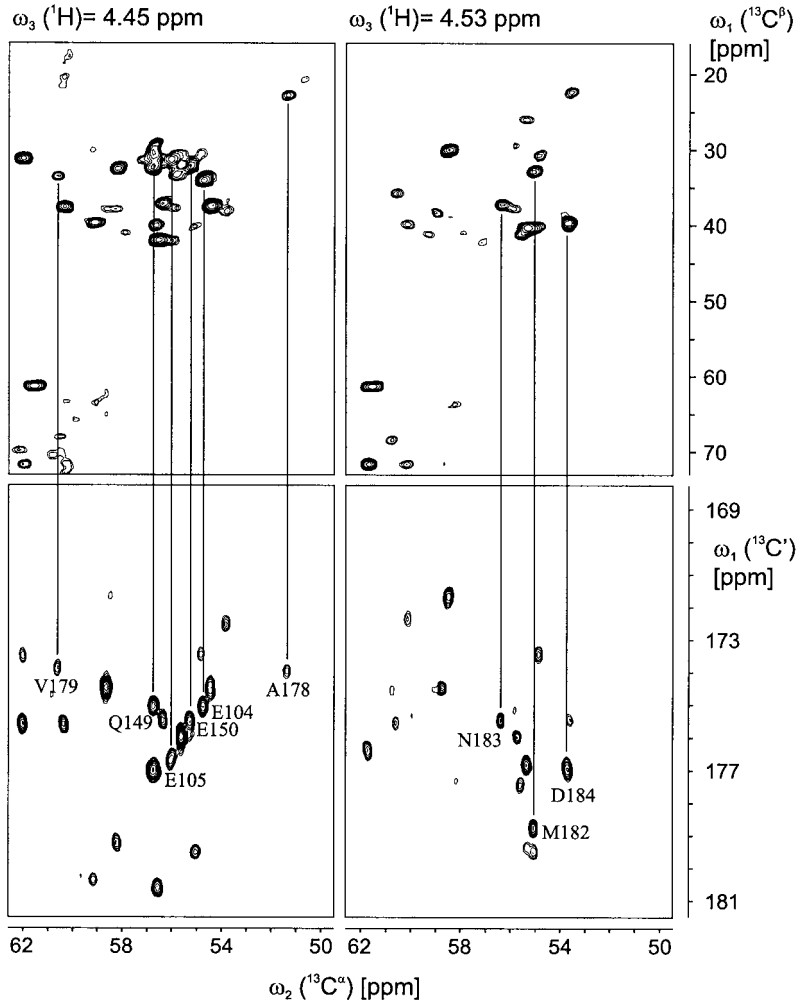

Figure 8. Expansions of ω_1/ω_2 planes from MQ-HCACB (top) and MQ-HCACO (bottom) spectra of DFPase, taken at two different $^1H^\alpha$ (ω_3) chemical shifts, as indicated above each panel. Only positive contour levels, spaced by a factor of $2^{1/2}$, are drawn. Intraresidual $^{13}C^\beta$-$^{13}C'$ connectivities of those residues discussed in the text are visualized by vertical lines.

was observed for each pair in the MQ-H(CA)NH, as is evident for Glu104/Glu105 in Figure 7. In case of the pairs Ala178/Val179 and Gln149/Glu150 the $^1H^\alpha$ degeneracy was aggravated by overlapping $^{13}C'$ and $^{13}C^\beta$ resonances, respectively. In the second example (at $\omega(^1H^\alpha) = 4.53$ ppm) MQ-HCACO and MQ-HCACB spectra were of particular importance for the assignment of the triplet Met182/Asn183/Asp184 which have almost identical $^1H^\alpha$ resonance frequencies, while no amide ^1H signal was detectable for Asn183 (see below), introducing a gap in the 'sequential walks' via intra- and interresidual ^{13}C to amide $^1H/^{15}N$ correlations. More generally, verifying $^{13}C'$, $^{13}C^\alpha$, $^{13}C^\beta$ and $^1H^\alpha$ assignments based on three independent ^{1}HN-detected experiments, i.e. HN(CA)CO (or (HCA)CO(CA)NH), HNCACB and MQ-H(CA)NH, MQ-HCACO and MQ-HCACB spectra added confidence to sequential connectivies previously identified.

Extent of resonance assignments for DFPase

The above described combination of $^1H^N$-based, [^{15}N,^1H]-TROSY type and $^1H^\alpha$-based, $^1H^\alpha/^{13}C^\alpha$ MQ methods enabled us to perform resonance assignments along the entire main chain of DFPase using a single $^1H^\alpha/^2H/^{13}C/^{15}N$-labelled sample. Only for Pro23, Pro36 and Pro270 no assignments were obtained. Excluding prolines, 98% of the main chain amide ^1H and ^{15}N signals were sequence-specifically assigned, the

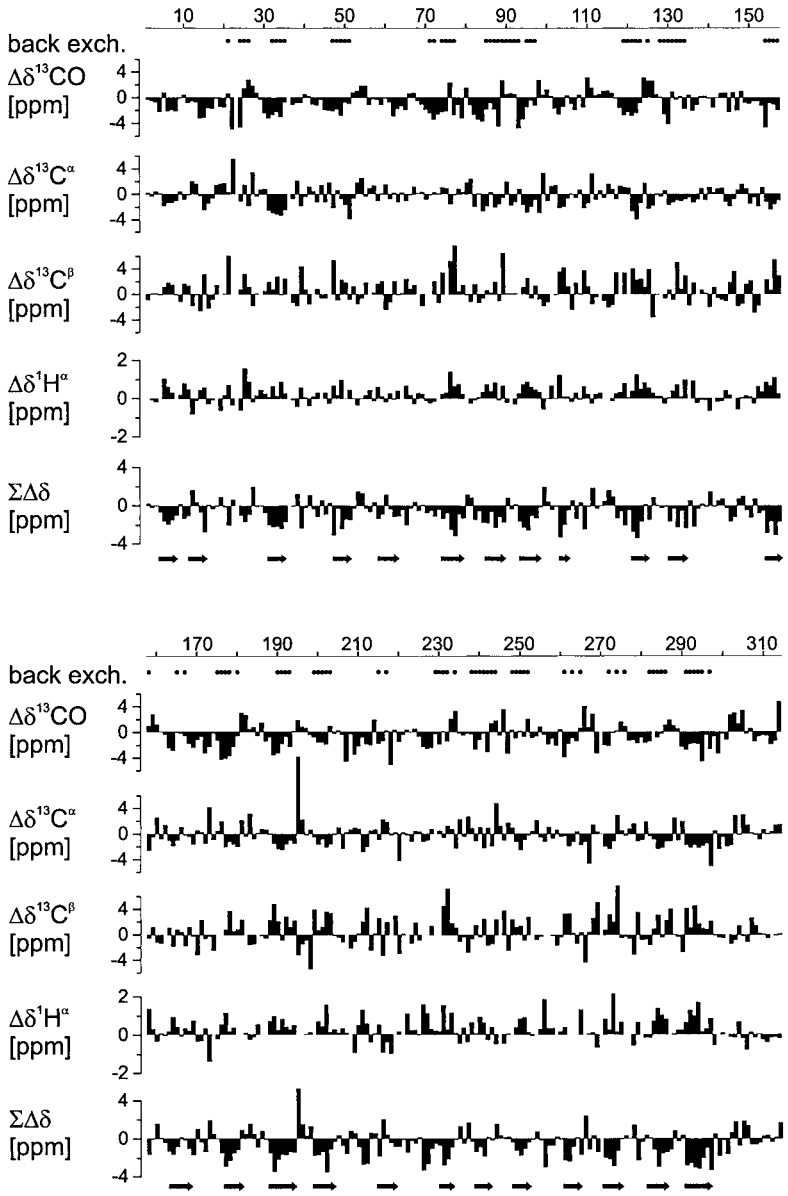

Figure 9. Secondary ^{13}CO, $^{13}C^{\alpha}$, $^{13}C^{\beta}$ and $^{1}H^{\alpha}$ chemical shifts of DFPase. The weighted consensus value ($\Sigma\Delta\delta$) was calculated as ($\Delta\delta\ ^{13}CO + \Delta\delta^{13}C^{\alpha} - \Delta\delta^{13}C^{\beta} - 4\Delta\delta^{1}H^{\alpha}$)/number of assignments per residue. Negative values are indicative of backbone conformation corresponding to β-sheets. Filled circles below the sequence numbering mark those residues that were unobservable in spectra of the perdeuterated protein due to very slow amide back-exchange. Horizontal arrows below the consensus secondary chemical shifts denote β-strands identified in the X-ray structure of DFPase (Scharff et al., 2001).

missing residues are Glu37, Asn41, Met148, Asn183 and Ser271, which did not give rise to detectable signals in ^{1}H, ^{15}N correlated spectra of either fully protonated, partially deuterated or perdeuterated DF-Pase. Possible reasons could be fast proton exchange with the solvent or excessive line broadening due to conformational exchange. Interestingly, Glu37 and Ser271 are located in the putative active site of the enzyme (Scharff et al., 2001), suggesting conformational disorder in the absence of a substrate. Likewise, $^{13}C^{\alpha}$ and $^{13}C^{\beta}$ of Asp229 as well as $^{13}C^{\beta}$ of Asn120 and Asn175, also part of the active site, were not observable. All remaining carbonyl, α- and β-carbon and 227 (67%) of the aliphatic side-chain ^{13}C res-

onances beyond C^{α} could be assigned. The number of $^{1}H^{\alpha}$ assignments amounts to 275 (88%), where the majority of the missing ones involves all proline (20), arginine (11), 3 out of 6 histidine residues and 3 out of 24 lysine residues. Assigned chemical shifts have been deposited at BioMagResBank (http:/www.bmrb.wisc.edu) under accession number 5618.

A graphical overview of the extent of $^{13}C'$, $^{13}C^{\alpha}$, $^{13}C^{\beta}$ and $^{1}H^{\alpha}$ assignments is given in Figure 9, showing the deviations of the chemical shifts from random coil values (Wishart et al., 1995). To avoid an influence of ^{2}H isotope effects on $^{13}C'$ and $^{13}C^{\alpha}$ secondary shifts the corresponding chemical shifts were extracted from [^{15}N,^{1}H]-TROSY-HNCO and [^{15}N,^{1}H]-TROSY-HNCA spectra, respectively, recorded on $^{13}C/^{15}N$-labelled DFPase. Differences between $^{13}C'$ chemical shifts in fully protonated and partially deuterated samples were found to be almost negligible (< 0.1 ppm) while they were in the range of 0.1–0.5 ppm for $\delta(^{13}C^{\alpha})$. It was not attempted to apply a correction for $^{13}C^{\beta}$ chemical shifts observed in the $^{1}H^{\alpha}/^{2}H/^{13}C/^{15}N$-labelled protein, based on empirical one-, two- and three-bond isotope shifts (Venters et al., 1996; Gardner et al., 1997), because the side-chain deuteration patterns were not exactly known here. However, for some residues $\delta(^{13}C^{\beta})$ values from $^{13}C/^{15}N$-labelled DFPase were available, revealing that these resonances are shifted upfield relative to a fully protonated sample by up to 1.0 ppm, depending on the residue type. The largest upfield shifts (i.e., > 0.8 ppm) were observed for arginine, proline, leucine, isoleucine, valine and methionine residues. Intermediate upfield shifts were found for aromatic as well as lysine, alanine, cysteine and serine residues while those of Glx, Asx and threonine residues were smaller than 0.2 ppm.

As shown by a recent crystal structure analysis (Scharff et al., 2001) DFPase exclusively contains β-sheets as secondary structure elements, arranged in a β-propeller fold. Positions of individual β-strands are in excellent agreement with the consensus secondary chemical shifts (Figure 9). Not unexpectedly, the vast majority of residues which could not be detected in spectra of perdeuterated DFPase are located in β-sheets, implying protection of amide protons from exchange with the solvent owing to hydrogen bonding.

Conclusions

It has been shown that the detrimental effect of very slow amide hydrogen exchange with the solvent for NMR studies on a deuterated protein can be circumvented by the use of a fully deuterated algal lysate in H_2O as the bacterial growth medium. Although the highest protonation levels are generally encountered at the C^{α} position, HN-based $^{13}C^{\alpha}$-relayed triple-resonance spectra of good quality can be obtained. Sensitivity enhancements owing to the deceleration of transverse relaxation afforded by deuteration are maintained to a high degree. Application of $^{1}H^{N}$-based, [^{15}N,^{1}H]-TROSY type in combination with $^{1}H^{\alpha}$-based, $^{1}H^{\alpha}/^{13}C^{\alpha}$ MQ triple resonance experiments made it possible to obtain essentially complete $^{1}H^{N}$, ^{15}N, $^{13}C'$, $^{1}H^{\alpha}$, $^{13}C^{\alpha}$ and $^{13}C^{\beta}$ assignments for a 314-residue protein.

Acknowledgements

The European Large Scale Facility for Biomolecular Magnetic Resonance at the University of Frankfurt is gratefully acknowledged for the use of its equipment.

References

Arrowsmith, C.H. and Wu, Y.-S. (1998) *Prog. Nucl. Magn. Reson. Spectrosc.*, **32**, 277–286.

Bax, A., Griffey, R.H. and Hawkins, B.L. (1983) *J. Magn. Reson.*, **55**, 301–315.

Bazzo, R., Cicero, D.O. and Barbato, G. (1995) *J. Magn. Reson.*, **B107**, 189–191.

Bendall, M.R., Pegg, D.T. and Doddrell, D.M. (1983) *J. Magn. Reson.*, **52**, 81–117.

Bodenhausen, G. and Ruben, D.J. (1980) *Chem. Phys. Lett.*, **69**, 185–189.

Boisbouvier, J., Gans, P., Blackledge, M., Brutscher, B. and Marion, D. (1999) *J. Am. Chem. Soc.*, **121**, 7700–7701.

Boucher, W., Laue, E.D., Campbell-Burk, S.L. and Domaille, P.J. (1992) *J. Biomol. NMR*, **2**, 631–637.

Boyd, J. and Soffe, N. (1989) *J. Magn. Reson.*, **85**, 406–413.

Carr, H.Y. and Purcell, E.M. (1954) *Phys. Rev.*, **94**, 630–638.

Clubb, R.T., Thanabal, V. and Wagner, G. (1992) *J. Magn. Reson.*, **97**, 213–217.

Constantine, K.L., Mueller, L., Goldfarb, V., Wittekind, M., Metzler, W.J., Yanchunas Jr, J., Robertson, J.G., Malley, M.F., Friedrichs, M.S. and Farmer II, B.T. (1997) *J. Mol. Biol.*, **267**, 1223–1246.

Czisch, M. and Boelens, R. (1998) *J. Magn. Reson.*, **134**, 158–160.

Delaglio, F., Grzesiek, S., Vuister, G.W., Zhu, G., Pfeifer, J. and Bax, A. (1995) *J. Biomol. NMR*, **6**, 277–293.

Deverell, C., Morgan, R.E. and Strange, J.H. (1970) *Mol. Phys.*, **18**, 553–559.

Dingley, A.J. and Grzesiek, S. (1998) *J. Am. Chem. Soc.*, **120**, 8293–8297.
Eletsky, A., Kienhöfer, A. and Pervushin, K. (2001) *J. Biomol. NMR*, **20**, 177–180.
Emsley, L. and Bodenhausen, G. (1990) *Chem. Phys. Lett.*, **165**, 469–476.
Farmer II, B.T. and Venters, R.A. (1995) *J. Am. Chem. Soc.*, **117**, 4187–4188.
Farmer II, B.T. and Venters, R.A. (1998) In *Biological Magnetic Resonance*, Vol. 16, Krishna, N.R. and Berliner, L.J. (Eds.), Kluwer Academic/Plenum Publishers, New York, NY, pp. 75–120.
Fiala, R., Czernek, J. and Sklenář, V. (2000) *J. Biomol. NMR*, **16**, 291–302.
Gardner, K.H. and Kay, L.E. (1998) *Annu. Rev. Biophys. Biomol. Struct.*, **27**, 357–406.
Gardner, K.H., Rosen, M.K. and Kay, L.E. (1997) *Biochemistry*, **36**, 1389–1401.
Geen, H. and Freeman, R. (1991) *J. Magn. Reson.*, **93**, 93–141.
Griffey, R.H. and Redfield, A.G. (1987) *Quart. Rev. Biophys.*, **19**, 51–82.
Grzesiek, S. and Bax, A (1992a) *J. Magn. Reson.*, **96**, 432–440.
Grzesiek, S. and Bax, A. (1992b) *J. Am. Chem. Soc.*, **114**, 6291–6293.
Grzesiek, S. and Bax, A. (1993a) *J. Biomol. NMR*, **3**, 185–204.
Grzesiek, S. and Bax, A. (1993b) *J. Am. Chem. Soc.*, **115**, 12593–12594.
Grzesiek, S. and Bax, A. (1995) *J. Biomol. NMR*, **6**, 335–339.
Grzesiek, S., Anglister, J., Ren, H. and Bax, A. (1993) *J. Am. Chem. Soc.*, **115**, 4369–4370.
Grzesiek, S., Kuboniwa, H., Hinck, A.P. and Bax, A. (1995) *J. Am. Chem. Soc.*, **117**, 5312–5315.
Günther, U.L., Ludwig, C. and Rüterjans, H. (2000) *J. Magn. Reson.*, **145**, 201–208.
Hartleib, J. and Rüterjans, H. (2001a) *Protein Expr. Purif.*, **21**, 210–219.
Hartleib, J. and Rüterjans, H. (2001b) *Biochim. Biophys. Acta*, **1546**, 312–324.
Hartleib, J., Geschwindner, S., Scharff, E.I. and Rüterjans, H. (2001) *Biochem. J.*, **353**, 579–589.
Heikkinen, S. and Kilpeläinen, I. (2001) *J. Magn. Reson.*, **151**, 314–319.
Ikura, M., Kay, L.E. and Bax, A. (1990) *Biochemistry*, **29**, 4659–4667.
Kay, L.E., Ikura, M. and Bax, A. (1991) *J. Magn. Reson.*, **91**, 84–92.
Kay, L.E., Keifer, P. and Saarinen, T. (1992) *J. Am. Chem. Soc.*, **114**, 10663–10665.
Kong, X.M., Sze, K.H. and Zhu, G. (1999) *J. Biomol. NMR*, **14**, 133–140.
Konrat, R., Yang, D. and Kay, L.E. (1999) *J. Biomol. NMR*, **15**, 309–313.
Kontaxis, G., Clore, G.M. and Bax, A. (2000) *J. Magn. Reson.*, **143**, 184–196.
Kupče, E.and Freeman, R. (1995) *J. Magn. Reson.*, **A115**, 273–276.
Kushlan, D.M. and LeMaster, D.M. (1993) *J. Biomol. NMR*, **3**, 701–708.
Larsson, G., Wijmenga, S. S. and Schleucher, J. (1999) *J. Biomol. NMR*, **14**, 169–174.
LeMaster, D.M. (1994) *Prog. Nucl. Magn. Reson. Spectrosc.*, **26**, 371–419.
LeMaster, D.M. and Richards, F.M. (1988) *Biochemistry*, **27**, 142–150.
Logan, T.M., Olejniczak, E.T., Xu, R.X. and Fesik, S.W. (1992) *FEBS Lett.*, **314**, 413–418.
Löhr, F. and Rüterjans, H. (1995a) *J. Biomol. NMR*, **6**, 189–197.
Löhr, F. and Rüterjans, H. (1995b) *J. Magn. Reson.*, **B109**, 80–87.
Löhr, F., Pfeiffer, S., Lin, Y.-J., Hartleib, J., Klimmek, O. and Rüterjans, H. (2000) *J. Biomol. NMR*, **18**, 337–346.
Loria, J.P., Rance, M. and Palmer III, A.G. (1999) *J. Magn. Reson.*, **141**, 180–184.
Marion, D., Ikura, M. and Bax, A. (1989a) *J. Magn. Reson.*, **84**, 425–430.
Marion, D., Ikura, M., Tschudin, R. and Bax, A. (1989b) *J. Magn. Reson.*, **85**, 393–399.
Markus, M.A., Dayie, K.T., Matsudaira, P. and Wagner, G. (1994) *J. Magn. Reson.*, **B105**, 192–195.
Matsuo, H., Kupče, E., Li, H. and Wagner, G. (1996) *J. Magn. Reson.*, **B111**, 194–198.
McCallum, S.A., Hitchens, T.K. and Rule, G.S. (1999) *J. Mol. Biol.*, **285**, 2119–2132.
McCoy, M.A. and Mueller, L. (1992) *J. Magn. Reson.*, **99**, 18–36.
Meiboom, S. and Gill, D. (1958) *Rev. Sci. Instrum.*, **29**, 688–691.
Mohebbi, A and Shaka, A.J. (1991) *Chem. Phys. Lett.*, **178**, 374–378.
Montelione, G.T. and Wagner, G. (1990) *J. Magn. Reson.*, **87**, 183–188.
Morris, G.A. and Freeman, R. (1979) *J. Am. Chem. Soc.*, **101**, 760–762.
Mulder, F.A.A., Ayed, A., Yang, D., Arrowsmith, C.H. and Kay, L.E. (2000) *J. Biomol. NMR*, **18**, 173–176.
Nietlispach, D., Clowes, R.T., Broadhurst, R.W., Ito, Y., Keeler, J., Kelly, M., Ashurst, J., Oschkinat, H., Domaille, P.J. and Laue, E.D. (1996) *J. Am. Chem. Soc.*, **118**, 407–415.
Palmer III, A.G., Cavanagh, J., Wright, P.E. and Rance, M. (1991) *J. Magn. Reson.*, **93**, 151–170.
Patt, S. (1992) *J. Magn. Reson.*, **96**, 94–102.
Pervushin, K., Riek, R., Wider, G. and Wüthrich, K. (1997) *Proc. Natl. Acad. Sci. USA*, **94**, 12366–12371.
Pervushin, K., Wider, G. and Wüthrich, K. (1998) *J. Biomol. NMR*, **12**, 345–348.
Powers, R., Gronenborn, A.M., Clore, G.M. and Bax, A. (1991) *J. Magn. Reson.*, **94**, 209–213.
Riek, R., Fiaux, J., Bertelsen, E.B., Horwich, A.L. and Wüthrich, K. (2002) *J. Am. Chem. Soc.*, **124**, 12144–12153.
Rosen, M.K., Gardner, K.H., Willis, R.C., Parris, W.E., Pawson, T. and Kay, L.E. (1996) *J. Mol. Biol.*, **263**, 627–636.
Salzmann, M., Pervushin, K., Wider, G., Senn, H. and Wüthrich, K. (1998) *Proc. Natl. Acad. Sci. USA*, **95**, 13585–13590.
Salzmann, M., Pervushin, K., Wider, G., Senn, H. and Wüthrich, K. (2000) *J. Am. Chem. Soc.*, **122**, 7543–7548.
Salzmann, M., Wider, G., Pervushin, K., Senn, H. and Wüthrich, K. (1999a) *J. Am. Chem. Soc.*, **121**, 844–848.
Salzmann, M., Wider, G., Pervushin, K. and Wüthrich, K. (1999b) *J. Biomol. NMR*, **15**, 181–184.
Salzmann, M., Pervushin, K., Wider, G., Senn, H. and Wüthrich, K. (1999c) *J. Biomol. NMR*, **14**, 85–88.
Sattler, M. and Fesik, S.W. (1996) *Structure*, **4**, 1245–1249.
Scharff, E.I., Koepke, J., Fritzsch, G., Lücke, C. and Rüterjans, H. (2001) *Structure*, **9**, 493–502.
Seip, S., Balbach, J. and Kessler, H. (1992) *J. Magn. Reson.*, **100**, 406–410.
Serber, Z., Ledwidge, R., Miller, S.M. and Dötsch, V. (2001) *J. Am. Chem. Soc.*, **123**, 8895–8901.
Shaka, A.J., Barker, P.B. and Freeman, R. (1985) *J. Magn. Reson.*, **64**, 547–552.
Shaka, A.J., Keeler, J., Frenkiel, T. and Freeman, R. (1983) *J. Magn. Reson.*, **52**, 335–338.

Shaka, A.J., Lee, C.J. and Pines, A. (1988) *J. Magn. Reson.*, **77**, 274–293.
Shan, X., Gardner, K.H., Muhandiram, D.R., Rao, N.S., Arrowsmith, C.H. and Kay, L.E. (1996) *J. Am. Chem. Soc.*, **118**, 6570–6579.
Stonehouse, J., Shaw, G.L., Keeler, J. and Laue, E.D. (1994) *J. Magn. Reson.*, **A107**, 178–184.
Swapna, G.V.T., Rios, C.B., Shang, Z. and Montelione, G.T. (1997) *J. Biomol. NMR*, **9**, 105–111.
Tessari, M., Gentile, L.N., Taylor, S.J., Shalloway, D.I., Nicholson, L.K. and Vuister, G.W. (1997) *Biochemistry*, **36**, 14561–14571.
Tugarinov, V., Muhandiram, R., Ayed, A. and Kay, L.E. (2002) *J. Am. Chem. Soc.*, **124**, 10025–10035.
Venters, R.A., Farmer II, B.T., Fierke, C.A. and Spicer, L.D. (1996) *J. Mol. Biol.*, **264**, 1101–1116.
Wang, Y.-X., Jacob, J., Cordier, F., Wingfield, P., Stahl, S.J., Lee-Huang, S., Torchia, D., Grzesiek, S. and Bax, A. (1999) *J. Biomol. NMR*, **14**, 181–184.
Weigelt, J. (1998) *J. Am. Chem. Soc.*, **120**, 10778–10779.
Wienk, H.L.J., Martínez, M.M., Yalloway, G.N., Schmidt, J.M., Pérez, C., Rüterjans, H. and Löhr, F. (2003) *J. Biomol. NMR*, **25**, 133–145.
Wishart, D.S., Bigam, C.G., Holm, A., Hodges, R.S. and Sykes, B.D. (1995) *J. Biomol. NMR*, **5**, 67–81.
Wittekind, M. and Mueller, L. (1993) *J. Magn. Reson.*, **B101**, 201–205.
Xia, Y., Kong, X., Smith, D.K., Liu, Y., Man, D. and Zhu, G. (2000) *J. Magn. Reson.*, **143**, 407–410.
Yamazaki, T., Lee, W., Arrowsmith, C.H., Muhandiram, D.R. and Kay, L.E. (1994) *J. Am. Chem. Soc.*, **116**, 11655–11666.
Yamazaki, T., Tochio, H., Furui, J., Aimoto, S. and Kyogoku, Y. (1997) *J. Am. Chem. Soc.*, **119**, 872–880.
Yang D. and Kay, L.E. (1999a) *J. Am. Chem. Soc.*, **121**, 2571–2575.
Yang, D. and Kay, L.E. (1999b) *J. Biomol. NMR*, **14**, 273–276.